

ど)に塗布し、貼布する。口腔～消化管のびらんも生じやすく、哺乳が障害されるため、輸液による栄養管理が必要である。発熱、CRP上昇はつねにある程度みられるが、敗血症をきたすと高熱、CRP高値となり、抗生物質加療が必要となる。低蛋白血症によりびらんは次第に遷延化し、腹水、胸水貯留、浮腫をきたす。残念ながら救命は困難である。本症は重篤で生命予後不良であるため、次子は出生前診断の適応となり、わが国でも慶應義塾大学、北海道大学などで施行可能である。


### 3. 栄養障害型表皮水疱症

最重症型のHallopeau-Siemens型では、びらん  
は難治性で生涯にわたり全身の包交を要する。  
シャワーでよく流したのち、軟膏を塗布した非  
固着性ガーゼや創傷被覆材（ハイドロコロイド、  
ポリウレタンフォーム、アルギン酸塩、ハイド  
ロファイバー・銀、ハイドロジェルなど）によ

り保護する。わが国では未承認であるが、  
Mepilex®は適度な密着性、粘着性と浸出吸収性  
があり、びらん面よりわずかに大きいサイズで  
貼布すると、使用感、治癒傾向ともによいとい  
う評価を得ている。摂食困難を伴うため、軟菜、  
粥とともにエンシュア・リキッド®などの総合  
栄養剤を併用する。手指の癒合については指間  
形成術を行うが、効果は限定的で再癒合は免れ  
ない。食道狭窄が強く、食物の通過障害をきた  
すようであれば食道拡張術を行う。びらんを繰  
り返した部位より有棘細胞がんを生じることが  
あり致命的となりうるため、発見次第、外科的  
切除を行う。本症も出生前診断の適応となる。

#### 著者連絡先

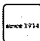
〒160-8582 東京都新宿区信濃町35  
慶應義塾大学医学部皮膚科学教室  
石河 晃



## 保険診療におけるカルテ記載のあり方 (改訂第3版)

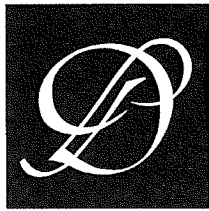
杏林大学医学部総合医療学講師 高木 泰 著

- A5判 108頁・定価2,625円(本体2,500円)税5% ISBN978-4-7878-1659-7
- カルテ開示時代における診療録の基本となる法的事項を具体的な記載例を紹介しながらやさしく解説した。第3版では、電子カルテ画面、DPCにおける留意点を追加、算定用件を差し替えた。



診断と治療社

〒100-0014 東京都千代田区永田町2-14-2 山王グランドビル4F  
電話 03(3580)2770 FAX 03(3580)2776  
<http://www.shindan.co.jp/> E-mail: [eigyobu@shindan.co.jp](mailto:eigyobu@shindan.co.jp)



◆特集／新しい皮膚科検査法 実践マニュアル

### Ⅲ. 皮膚病理学検査法 電子顕微鏡による検査法 —免疫電顕を含めて—

石河 晃\*

**Key words :** 電子顕微鏡 (electron microscopy), 免疫電顕 (immunoelectron microscopy), CADASIL, 表皮水疱症 (epidermolysis bullosa), 基底膜部 (basement membrane zone)

**Abstract** 電子顕微鏡はウルトラミクロの病理診断学として重要であり, 皮膚科医が電顕用検体を提出する際の要点をまとめた. ポイントは観察可能な範囲が極めて小さいことであり, 1つの標本には1つの目的をもって提出することが肝要である. 無色素性悪性黒色腫, メルケル細胞癌などの腫瘍性疾患の診断, 表皮水疱症, CADASIL などの遺伝性疾患の診断には電顕病理学は特に有用である. また, 眼皮膚白皮症では電顕 DOPA 反応によりチロジナーゼ陽性・陰性を判定することが可能であり, 異物沈着症の異物同定にはX線元素分析が有用である. さらに, 免疫電顕法の進歩により抗原蛋白の局在や, 未知であった構造物の組成を示すこともできる. 分子生物学の進歩と相まって *in vitro* における知見を *in vivo* の微細形態に落とし込むためのツールとして電顕の役割は重要である.

#### はじめに

最初の電子顕微鏡 (TEM) は 1931 年にベルリン工科大学のマックス・クノールとエルンスト・ルスカが開発した. 以来, 生物学では細胞小器官, 微細構造が明らかにされ, 医学ではさまざまな病態におけるそれらの微細変化が解明されてきた. 1980 年代には免疫電顕が導入され, 蛋白分子の超微細局在を電顕レベルで示すことが可能となった. 本稿ではまず, 電子顕微鏡検査に必要な標本作製方法を概説し, 皮膚科学における電子顕微鏡の応用につき述べる.

#### 電顕標本作製に必要な知識

##### 1. 検体採取, 固定にあたって

通常の透過型電子顕微鏡による組織観察にあたり, 最低限知っておきたいことを簡潔に述べる. 検体を提出する皮膚科医として電顕で観察できる

範囲は極めて小さいことを常に意識しておく必要がある. 通常の光学顕微鏡観察のように正常部位と病変部位を両方含むような検体提出は望ましくない. 正常部との比較が必要な場合は, 正常部と病変部の2種類のサンプルを別々に提出すべきである. 病変部は中央部を「どこを切っても病変部」であるように提出することが肝要である. 電顕固定液は強力であり, 表面が早く固定され, 深い所は固定が届かないことがあるため, 提出標本は 2 mm 以下にしておく. 大きめの標本を数分間固定液に入れておいてから, 必要な部分を 2 mm 大に切り出すのがやりやすい. 固定液は通常は 4°C にあらかじめ冷却した 2% グルタルアルデヒド / 60 mM Hepes buffer を用いている.

診断困難が予測される症例にはあらかじめ電顕ブロックを作製しておくことを推奨するが, 万一, 切除時にすべてホルマリン固定してしまっている場合, ホルマリン固定で止まっている組織があればそこから電顕固定をし直し, 通常の電顕標本作製過程にのせることでかなり解像度のよい電顕像が得られる. パラフィン包埋までされてしまっ

\* Akira ISHIKO, 〒160-8582 東京都新宿区信濃町 35 慶應義塾大学医学部皮膚科学教室, 准教授

表 1. 透過電子顕微鏡標本作製法

1. 2 mm 以下に標本を細切
2. 2%グルタルアルデヒド/Hepes 緩衝液にて4℃, 2時間以上固定
3. 1%オスミウム酸/Hepes 緩衝液にて4℃, 2時間固定
4. 50%エタノール 5分
5. 70%エタノール 20分
6. 80%エタノール 20分
7. 90%エタノール 20分
8. 95%エタノール 20分
9. 100%エタノール 20分
10. 100%エタノール 20分
11. アセトン 30分
12. アセトン+QY(1:1) 30分
13. QY 30分
14. QY 30分
15. QY+Epon812(1:1) 1時間
16. Epon812 3時間
17. Epon 包埋, 55℃ 3日以上

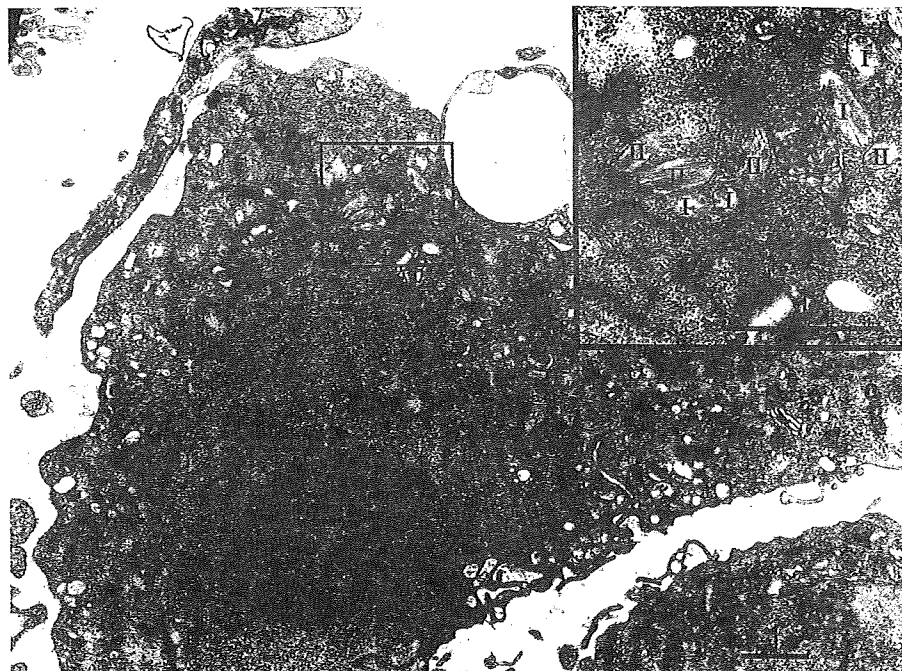


図 1. 紅色有形性腫瘍を呈した無色素性悪性黒色腫の電顕像  
成熟メラノソーム(IV型)は全くみられない。未熟なメラノソーム(挿入図にI型およびII型を示す)がみられることからメラノーマであることが分かる。(スケールバー:1 μm)

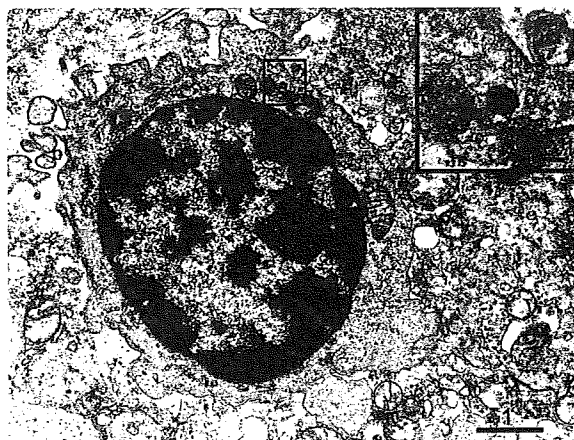


図 2. 顔面に生じたメルケル細胞癌の電顕像  
ヘテロクロマチンに富む円形の核を有する小型の細胞で、挿入図に有芯顆粒(dense core granule)を示す。  
(スケールバー:1 μm, 0.1 μm)

久的に保存可能である。ブロックから硝子ナイフを用いて顕微鏡用の厚切り切片(1 μm)を作製し、トルイジンブルー染色を施し全体像を光学顕微鏡で観察する。電顕で観察したい部位を0.5 mm角にトリミングし、ダイヤモンドナイフを用いて超薄切片(0.07 μm程度)を作製、グリッドに乗せ酢酸ウラン、クエン酸鉛溶液で電子染色を施し観察する。

### 皮膚の電顕で分かること

#### 1. 腫瘍の診断

腫瘍、特に悪性腫瘍はその起源となる細胞の特徴を電子顕微鏡下にとらえることにより診断に迫ることが可能である。特殊染色が染まらないときなど細胞起源を探るのに有用である。血管内皮細胞のWibel-Palade顆粒、メラノサイトのメラニン顆粒、上皮系腫瘍のデスモソーム、メルケル細胞の有芯顆粒、ランゲルハンス細胞のBirbeck顆粒などは診断価値が高い。図1に無色素性悪性黒色腫の電顕像、図2にメルケル細胞癌の電顕像を示す。それぞれ未熟なメラノソーム、有芯顆粒が診断根拠となった。

いる場合は厚切り切片を脱パラフィンし、親水化した後、電顕固定してゆくいわゆる「戻し電顕」を考慮するが、微細形態の詳細な評価は困難である。

#### 2. 標本作製にあたって

標本作製の詳細は専門書<sup>1)</sup>にゆだねるが、概略を表1に示す。ブロックまで作製しておけば半永

図 3.  
 栄養障害型表皮水疱症の水疱辺縁部の電顕像  
 水疱(\*)は基底板(LD)より真皮側に形成されている。挿入図は正常の基底膜部電顕像を示す。  
 TF: トノフィラメント, HD: ヘミデスモソーム, PM: 細胞膜, LL: 透明層, Af: 係留細線維, LD: 基底板, AF: 係留線維, CF: 膠原線維 (スケールバー: 1 μm)

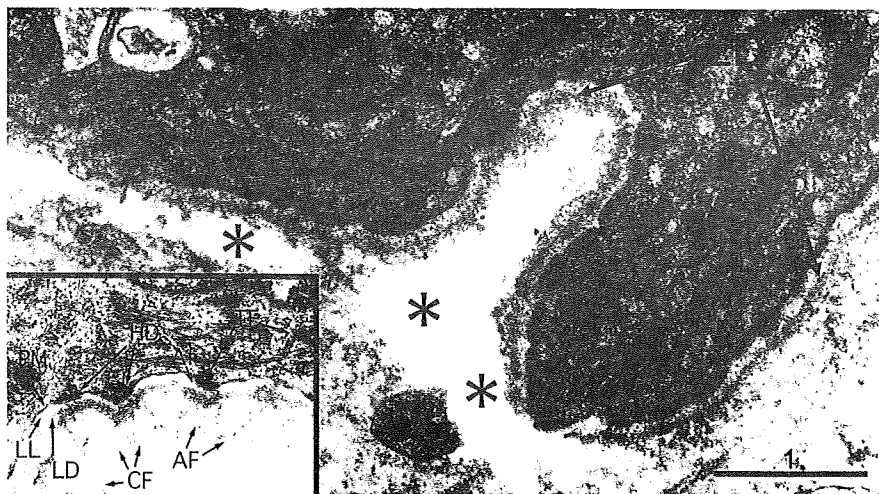
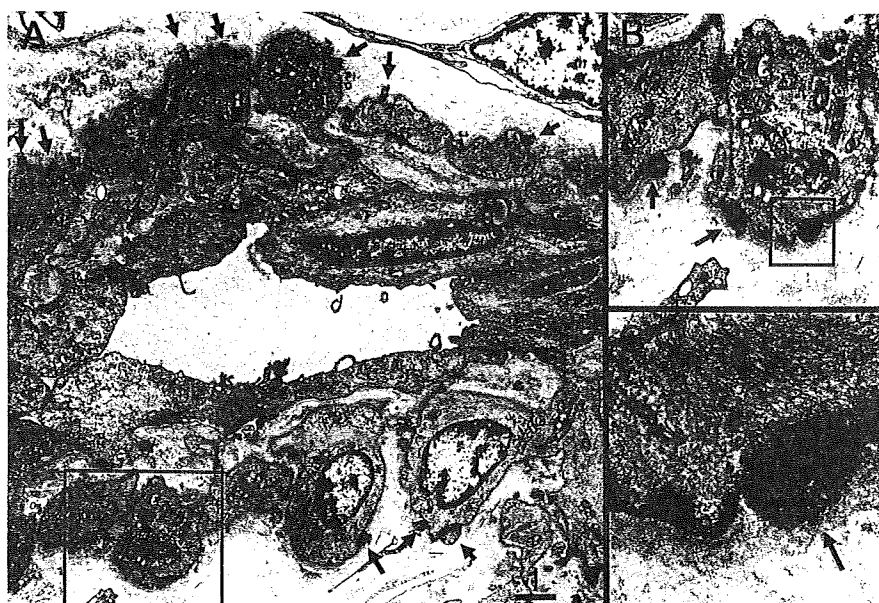


図 4.  
 若年性の遺伝性脳血管障害であるCADASIL患者の正常にみえる皮膚を生検した組織の電顕像  
 Aは真皮深層の最小動脈全体像, BはAの栓組部の拡大, CはBの栓組部の拡大である。矢印に電子密度の高い沈着物GOMを示す。血管平滑筋の外周に食い込むように存在している。(スケールバー: 1 μm)



## 2. 遺伝性疾患の診断

皮膚科で扱う遺伝性疾患は、ケラチンやⅦ型コラーゲンなどの構造蛋白の異常によるものとチロジナーゼやαガラクトシダーゼなどの酵素異常によるものが多い。いずれの異常においても微細形態に変化がみられることが多く、電顕的解析により確定診断、病型分類がなされることがある。

先天性表皮水疱症は、表皮基底膜部蛋白の遺伝子異常により生じる。水疱が生じる部位の深さにより、表皮内に生じる単純型、表皮真皮接合部に水疱を生じる接合部型、基底板直下の真皮内に水疱を生じる栄養障害型に大別される<sup>2)</sup>。その水疱形成部位と、責任遺伝子、臨床症状の間には密接

な関連があり、電顕的所見が診断に重要である<sup>3)</sup>。基底膜部構成蛋白に対するモノクローナル抗体を用いて患者皮膚における蛋白発現異常を検出することと遺伝子診断により病型が確定する。図3にⅦ型コラーゲン欠損により発症した劣性栄養障害型表皮水疱症の電顕像を示す。Ⅶ型コラーゲンが主成分である係留線維はほとんどみられず、水疱は基底板直下に生じていることから栄養障害型表皮水疱症であることが診断された。

CADASIL (cerebral autosomal dominant arteriopathy with subcortical infarcts and leukoencephalopathy)は若年で脳虚血発作を繰り返し、痴呆、死亡に至る稀な遺伝性疾患であり、Notch3 遺

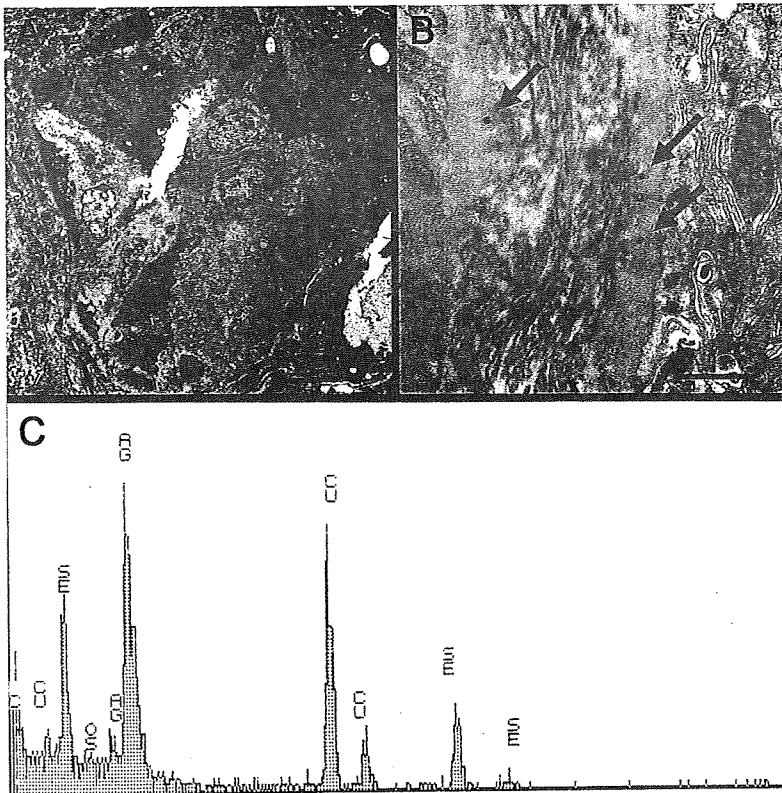


図 5.  
顔面の青黒色調色素沈着をきたした銀皮症  
患者皮膚の汗腺分泌部電顕像  
B は A の枠組部の拡大である。矢印に汗  
腺基底膜に沈着した電子密な顆粒を示す。  
この部分の X 線元素分析(C)により銀、セ  
レン、銅が検出された。銅は標本を乗せて  
いるグリッド由来であるため、沈着物はセ  
レン化銀であると同定された。  
(スケールバー：5  $\mu\text{m}$ , 1  $\mu\text{m}$ )

伝子の変異により発症する。皮膚は全く無症状であるが、電顕で生検皮膚の血管平滑筋を観察することで診断が可能である<sup>4)</sup>ことから皮膚科医も知っておくべき疾患である。頭部 MRI 所見は大脳皮質病変の欠如と前頭側頭葉優位の白質病変の存在が特徴で、大脳基底核、視床、大脳白質などにラクナ梗塞が多発し、かつ白質脳症を伴う。電顕所見は血管平滑筋周囲に GOM (granular osmiophilic material) と呼ばれる物質が沈着することが特徴である。

GOM は微細な顆粒状物質の集合体で、200~800 nm の大きさを持つ。細胞膜と 10~30 nm ほどの間隔をもち、膜に近いほど密度が高い(図 4)。GOM の存在は CADASIL 診断において極めて特異的であり、種々の報告でも 100% の特異性を有する。診断のための皮膚生検は体中どこ部位でもよいが、細動脈をみるため真皮深層を含むことが条件である。皮膚科医が生検から電顕観察までを担当するのが理想的であるが、電顕検査を外注する場合には、真皮皮下組織境界部の小動脈もしくは汗腺周囲の細小動脈が含まれる切片作製を依

頼し、血管平滑筋細胞をターゲットとして写真を撮ることを依頼することが肝要である。

### 3. 元素分析

異物沈着が疑われるとき、電顕を用いた X 線微小解析は異物を構成する元素を同定する際に有力な武器となる。刺青、外傷性刺青、銀皮症など、微小な異物を同定できる。図 5 は銀皮症の患者皮膚の汗腺基底膜部に沈着した粒子を示すが、セレンと銀が解析により検出された。生体内では化学的に非常に安定なセレン化銀として長年にわたり沈着し続けることが分かる<sup>5)</sup>。検体は通常の電顕切片を電子染色せずに観察し、目標の異物に X 線を当てる。通常の電子顕微鏡に加え解析装置が必要である。

### 4. 酵素組織化学

光学顕微鏡と同様に酵素組織化学を電顕上で行うことが一部可能である。DOPA 反応はチロジナーゼの基質である DOPA を反応させることによりその酸化物が黒色に観察されるものであるが、電顕的にも電子密物質として観察されるため、チロジナーゼを有する未熟のメラノソームが染色

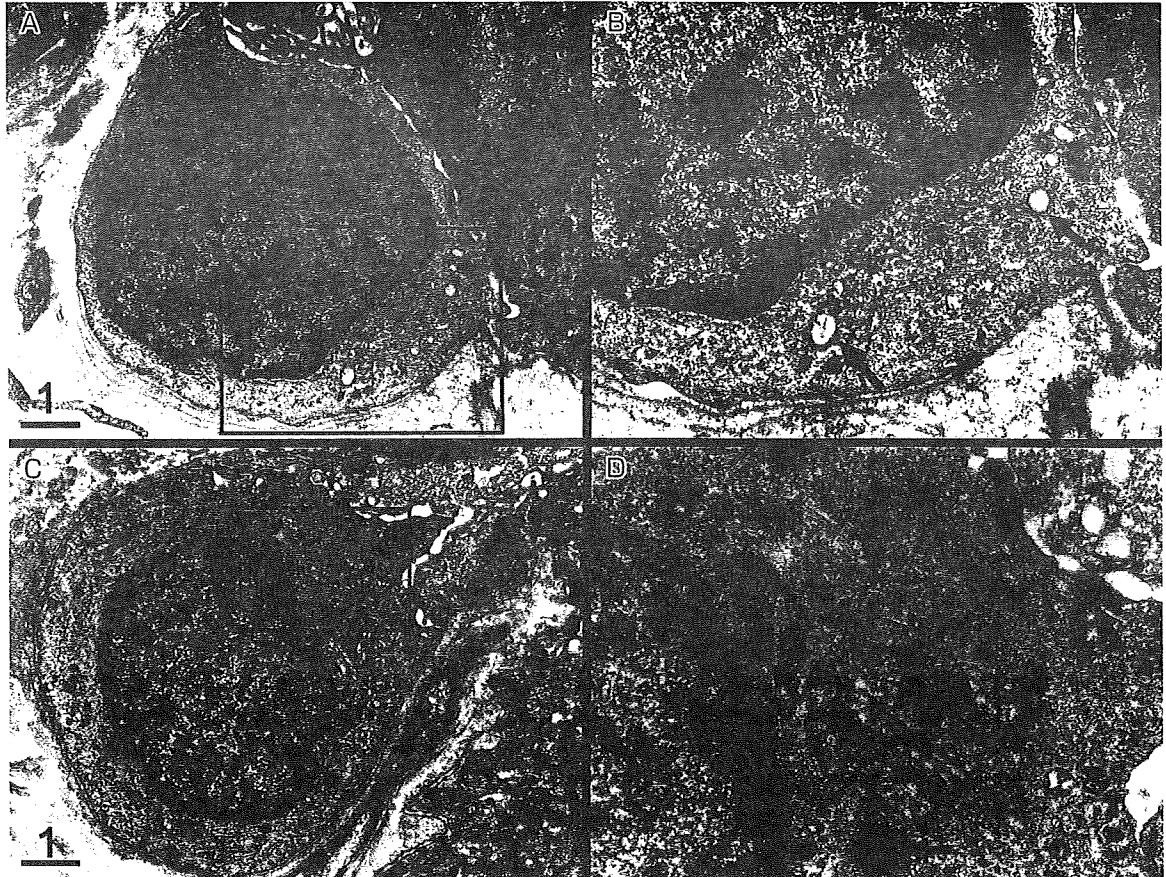


図 6. 眼皮膚白皮症患者のメラノサイト電顕像(A, B)とDOPA電顕像(C, D)

BはAの枠組部の拡大, DはCの枠組部の拡大である. 通常電顕ではメラノソーム(矢印)の同定は困難であるが, DOPA反応後の電顕像では明らかに円形のメラノソームが黒染され(矢印), チロジナーゼの欠損はないことが証明される. (スケールバー: 1  $\mu$ m)

される. 白皮症のチロジナーゼ陽性型・陰性型の判別<sup>6)</sup>や無色素性悪性黒色腫の診断に用いられる. 図6に眼皮膚白皮症の患者皮膚のメラノサイト電顕像とDOPA電顕像を示す. 通常電顕では黒色のメラノソームはほとんどみられないが, DOPA反応後には未熟なメラノソームが黒染され, チロジナーゼを含有していることが確認された.

### 5. 免疫電顕

光顕用切片で免疫組織染色を行うのと同じように電子顕微鏡レベルで免疫組織染色を行うことができる. しかし, 通常の固定, 包埋法では抗原性が失活してしまうため, 工夫が必要である. 最も簡単な方法は組織を固定する前に, 標本を丸ごと抗体と反応させて, 免疫染色を済ませてから通常の電顕固定, 包埋を行い, 電顕で観察する方法で

ある(包埋前免疫染色法). しかしこの方法では抗体が浸透しにくい細胞内部や小器官内部は偽陰性となってしまう, 真の抗原分布とはかなり差がある可能性が高い. 理想的な免疫染色のためには切片にしてから免疫反応をすべきである. これを可能にした技術の一つが凍結固定・凍結置換法である. これは化学固定液を用いず, 組織を $-190^{\circ}\text{C}$ に冷却した液体プロパンに急速挿入し無晶凍結(氷の結晶が微細形態を破壊するのを防ぐ)し,  $-80^{\circ}\text{C}$ の低温下でメタノールやアセトンなどの溶媒と置換脱水し,  $-60^{\circ}\text{C}$ の低温下で液状を保つ特殊樹脂Lowicryl K11 Mに包埋し, 紫外線照射にて樹脂を重合させてから室温に戻す方法である. これにより組織は化学固定液や熱にさらされることなく樹脂の中に固められるわけである(包埋後免疫染色法). 作製したブロックから超薄切片を

表 2. 凍結固定・凍結置換法

1. 組織採取後直ちに 15%グリセリン/PBS に入れ 4℃ に冷却
2. 0.5 mm 角にトリミング
3. -190℃ 液体プロパンに 3 m/s 以上の速度で挿入
4. -80℃ メタノールに 48 時間置換
5. -60℃ Lowicryl K11 M 樹脂(液体)に置換, 包埋
6. -60℃ 紫外線重合 3 日間以上
7. 室温まで上昇させ, さらに紫外線重合を続ける
8. 超薄切片作製
9. ゼラチン・BSA・正常ヤギ血清含有緩衝液にて非特異反応ブロック
10. 1 次抗体, 室温 2 時間
11. 緩衝液にて洗浄
12. 2 次抗体(金コロイド標識ヤギ抗体), 室温 2 時間
13. 緩衝液にて洗浄
14. 水洗
15. 電子染色
16. 水洗
17. 乾燥
18. 電顕観察

切り出し, 切片上で免疫染色を行う。この方法の最大のメリットは, 抗原の解剖学的位置にかかわらず, 切片表面に露出したすべての抗原を抗体浸透度に関係なく検出できること, また, 抗体の標識に 5 nm の金コロイド粒子を用いることで抗原量を半定量できることである。デメリットは特殊な機材と技術を要する点である。表 2 に具体的な手順を示す。

#### 臨床応用例

水疱性類天疱瘡 (BP), 後天性表皮水疱症 (EBA), 抗 p200 類天疱瘡 (p200 BP) はいずれも表皮下に水疱を形成する自己免疫性水疱症であり, 蛍光抗体直接法にて表皮基底膜部に IgG 自己抗体の沈着がみられる。しかしながら, 自己抗体の標的抗原はそれぞれ BPAG1/BPAG2, VII 型コラーゲン, 未知の 200 kDa 蛋白であり, 免疫ブロット法などの解析を行わないと鑑別が困難である。しかし, 包埋後免疫染色法と金コロイドをプローブとした免疫電顕間接法を施行すると図 7のごとく, 標的抗原の局在の差が明らかになる。すなわち, 患者血清を正常ヒト皮膚(免疫電顕用切片)と反応させ, 抗原と結合した IgG を 5 nm 金コロイド標識抗ヒト IgG ヤギ抗体を用いて検出

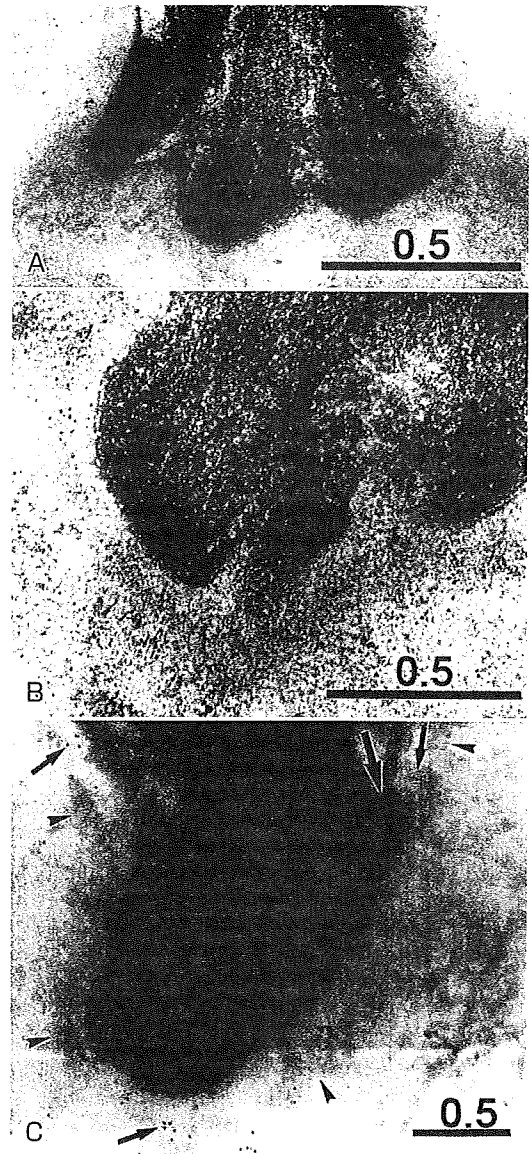


図 7. 水疱性類天疱瘡 (A), 後天性表皮水疱症 (B), 抗 p 200 類天疱瘡 (C) の免疫電顕所見  
 黒色の顆粒が抗体の標識に用いた金コロイドである。A ではヘミデスモソームの細胞膜に沿って, B では基底膜に沿って, C では透明層の基底膜近くに標的抗原があることが明らかである。A, B は包埋後染色法, C は凍結超薄切片法。  
 (スケールバー: 0.5  $\mu$ m)

すると, BP では基底細胞膜のヘミデスモソームに沿った BPAG2 の抗原分布がみられるが<sup>7)</sup>, EBA では基底細胞膜より離れた基底膜内に分布する VII 型コラーゲン C 末端部位がラベルされる<sup>8)</sup>。一方, p200 BP では基底細胞膜と基底膜の間に存在する透明層の基底膜よりに抗原がみられる<sup>9)</sup> (図 7)。

## 研究への応用

前述した CADASIL でみられる血管平滑筋周囲に沈着する GOM の正体は長らく不明であったが、Notch3 蛋白の細胞外ドメインを認識する抗体と細胞内ドメインを認識する抗体それぞれを用いて免疫電顕で観察することにより、GOM の主成分は Notch3 蛋白の細胞外ドメインであることが明らかになった<sup>10)</sup>。このように免疫電顕は形態学的な異常と蛋白の異常、ひいては遺伝子の異常を結びつける有力な方法である。また、1つの蛋白に対しいくつかのエピトープ特異的抗体の結合部位を同定することにより、かなり詳細に蛋白の形状、方向などをトレースすることも可能である。

## 最後に

皮膚科の発疹学はマクロ形態学にはかならない。ダーモスコピーはサブミクロ形態学であり、悪性黒色腫や基底細胞癌などの腫瘍診断に画期的な進歩をもたらした。病理組織学はミクロ形態学であり、皮膚科の診断には不可欠なものである。電顕組織学はウルトラミクロの形態学である。しかし、生物学が細胞から分子へ、遺伝子へと解析法が発展するにつれ、遺伝子異常がウルトラミクロに及ぼす影響が無視できないことが表皮水疱症や CADASIL をみても明らかとなってきた。分子生物学の進歩と関連した超微細形態の変化、その病態に及ぼす影響を常に意識することが重要であり、これを可能にする方法が電顕形態学、免疫電顕である。今後、電子顕微鏡的解析は分子生物学・遺伝子生物学と *in vivo* の形態学との懸け橋として役割を果たしてゆくことと思われる。

## 文 献

1) 日本顕微鏡学会(編)：電顕入門ガイドブック，学

会出版センター，2004.

- 2) Fine JD, Eady RA, Bauer EA et al: The classification of inherited epidermolysis bullosa (EB) : Report of the Third International Consensus Meeting on Diagnosis and Classification of EB [In Process Citation]. *J Am Acad Dermatol*, 58 : 931-950, 2008.
- 3) 石河 晃：表皮接着分子構造と水疱症水疱形成部位と接着分子. *MB Derma*, 137 : 1-9, 2008.
- 4) Ishiko A, Shimizu A, Nagata E et al: Cerebral autosomal dominant arteriopathy with subcortical infarcts and leukoencephalopathy (CADASIL) : a hereditary cerebrovascular disease, which can be diagnosed by skin biopsy electron microscopy. *Am J Dermatopathol*, 27 : 131-134, 2005.
- 5) 吉田理恵, 石河 晃, 清水 篤ほか：仁丹による銀皮症. *皮膚病診療*, 26 : 313-316, 2004.
- 6) Takizawa Y, Kato S, Matsunaga J et al: Electron microscopic DOPA reaction test for oculocutaneous albinism. *Arch Dermatol Res*, 292 : 301-305, 2000.
- 7) Ishiko A, Shimizu H, Kikuchi A et al: Human autoantibodies against the 230-kD bullous pemphigoid antigen (BPAG1) bind only to the intracellular domain of the hemidesmosome, whereas those against the 180-kD bullous pemphigoid antigen (BPAG2) bind along the plasma membrane of the hemidesmosome in normal human and swine skin. *J Clin Invest*, 91 : 1608-1615, 1993.
- 8) Ishiko A, Hashimoto T, Shimizu H et al: Epidermolysis bullosa acquisita : report of a case with comparison of immunogold electron microscopy using pre- and postembedding labelling. *Br J Dermatol*, 134 : 147-151, 1996.
- 9) Chen KR, Shimizu S, Miyakawa S et al: Coexistence of psoriasis and an unusual IgG-mediated subepidermal bullous dermatosis : identification of a novel 200-kDa lower lamina lucida target antigen. *Br J Dermatol*, 134 : 340-346, 1996.
- 10) Ishiko A, Shimizu A, Nagata E et al: Notch3 ectodomain is a major component of granular osmiophilic material (GOM) in CADASIL. *Acta Neuropathol*, 112 : 333-339, 2006.





## Subcellular localization of desmosomal components is different between desmoglein3 knockout mice and pemphigus vulgaris model mice

Hitoshi Saito<sup>a,b</sup>, Atsushi Shimizu<sup>b</sup>, Kazuyuki Tsunoda<sup>b</sup>, Masayuki Amagai<sup>b</sup>, Akira Ishiko<sup>b,\*</sup>

<sup>a</sup> Department of Dermatology, Saitama Municipal Hospital, 2460 Mimuro, Midori-ku, Saitama-shi, Saitama 336-8522, Japan

<sup>b</sup> Department of Dermatology, Keio University School of Medicine, 35 Shinanomachi, Shinjuku-ku, Tokyo 160-8582, Japan

### ARTICLE INFO

#### Article history:

Received 31 July 2008

Received in revised form 2 March 2009

Accepted 17 May 2009

#### Keywords:

Desmosome

Immunogold

Electron microscopy

Adhesion molecule

Autoimmune

Ultrastructural localization

### ABSTRACT

**Background:** The Desmoglein 3 (Dsg3) knockout mouse and pemphigus vulgaris (PV) mouse model present a similar type of supra-basal acantholysis, even though the subcellular mechanism is considered to be completely different.

**Objectives:** To detect changes in the desmosomal molecular composition in Dsg3<sup>-/-</sup> mice and PV model mice to highlight the precise mechanism for acantholysis at an ultrastructural level.

**Methods:** Using epithelia from Dsg3<sup>-/-</sup> mice, PV model mice, and their respective control mice, the desmosomal components were immunostained using a post-embedding immunogold labeling method, and their precise localization and the labeling density were statistically analyzed in the desmosomes before the occurrence of acantholysis.

**Results:** Positive findings were detected in desmoplakin and plakoglobin. In the Dsg3<sup>-/-</sup> mice, the localization of desmoplakin shifted 12.6 nm toward the cytoplasm and the plakoglobin labeling density per desmosome decreased 31% in the desmosomes. In the PV model mice Desmoplakin shifted 22.7 nm more distantly from the plasma membrane but the labeling density per desmosome showed no significant difference, including plakoglobin. Similar results were obtained when analyzing the desmosomes of spinous cells in the mid-epidermis.

**Conclusion:** These results showed the functional blocking of Dsg3 by autoantibody binding and the genetic defect of Dsg3 to induce different changes in the cytoplasmic desmosomal plaque proteins. A decrease in the level of plakoglobin is therefore not involved in the acantholysis in the PV model mice. The desmoplakin shift from the desmosomal plaque, which is induced by autoantibody binding under *in vivo* conditions in the PV model mouse, could be an early molecular change before the occurrence of acantholysis.

© 2009 Japanese Society for Investigative Dermatology. Published by Elsevier Ireland Ltd. All rights reserved.

### 1. Introduction

Desmoglein3 (Dsg3) is a transmembrane desmosomal component that belongs to the cadherin supergene family and is a target antigen of pemphigus vulgaris (PV), a severe autoimmune blistering skin disease [1,2]. Knockout mice of this molecule (Dsg3<sup>-/-</sup>) present erosions on the mucous membrane with suprabasal acantholysis, which is a characteristic pathological feature of human PV [3]. On the other hand, an experimental mouse active model for PV with circulating autoantibodies against Dsg3 has been established [4,5]. Both Dsg3<sup>-/-</sup> mice and PV model mice present a similar human PV-like phenotype clinically and histologically [3–5]. Furthermore, the ultrastructural features of

the Dsg3<sup>-/-</sup> mice and the PV model mice are strikingly similar and parallel to those of PV patients [6], although the start point of the cause for acantholysis is essentially different between the two mice. Therefore a more precise analysis is needed at the molecular level to distinguish the subcellular mechanism for acantholysis in these mice.

Currently, the possible mechanisms for acantholysis in PV include: (1) interference of desmosomal cadherin induced by intracellular changes that occur subsequently to autoantibody binding, (2) direct inhibition of the extracellular Dsg3 adhesive ability by autoantibody binding to Dsg3 (steric hindrance), (3) decrease of Dsg3 from desmosomes. Recent studies have speculated that either one of these alone might not be sufficient to explain the acantholysis in PV [7–9].

The purpose of this study is to detect changes in the desmosomal molecular composition in Dsg3<sup>-/-</sup> mice and PV model mice in order to give insight into the mechanisms of

\* Corresponding author. Tel.: +81 3 3353 1211; fax: +81 3 3353 6880.  
E-mail address: [ishiko@sc.itc.keio.ac.jp](mailto:ishiko@sc.itc.keio.ac.jp) (A. Ishiko).

acantholysis in each mouse in order to obtain a better understanding of PV acantholysis.

## 2. Material and methods

### 2.1. Mice

#### 2.1.1. Dsg3 knockout mice

Dsg3<sup>-/-</sup> mice were obtained by mating male Dsg3<sup>-/-</sup> and female Dsg3<sup>+/-</sup> mice (Jackson Laboratory, Bar Harbor, Maine, USA) [3]. Dsg3<sup>-/-</sup> mice had been crossed with C57BL/6, but had, strictly speaking, a mixed genetic background of 129/SV and C57BL/6J (H-2b) mice. Due to the fact that we could not obtain their littermates, C57BL/6 mice were used as controls, although there might be a possibility to have a small anatomical difference. This study used Dsg3<sup>-/-</sup> mice at 13 weeks of age and C57BL/6 mice at 20 weeks of age, both of which were young adult mice.

#### 2.1.2. PV model mice

PV model mice were obtained as described previously [4]. In brief, Dsg3<sup>-/-</sup> mice, which did not have immunological tolerance to Dsg3, were immunized with recombinant mouse Dsg3 and their splenocytes were transferred to 7-week-old C57BL/6 Rag2<sup>-/-</sup> mice that had been backcrossed to B6SJLPtcrca mice for ten generations (Taconic Farms, Germantown, NY, USA) [10]. The Rag2<sup>-/-</sup> mice produced anti-Dsg3 autoantibodies continuously and showed erosions in the oral mucous membranes and patchy hair loss 15–25 day after the transfer. The immuno-EM study was duplicated using two PV model mice at 16 weeks of age. C57BL/6 Rag2<sup>-/-</sup> mice at 13 weeks of age that also had been backcrossed to B6SJLPtcrca mice were used as controls.

In order to detect the initial ultrastructural changes in the desmosomes, the samples were taken from the oral mucous membrane where neither blistering nor erosion was seen in both Dsg3<sup>-/-</sup> and PV model mice.

### 2.2. Antibodies

Seven antibodies against major desmosomal components were used in this study; (1) rabbit polyclonal antibodies to desmoplakin (Dp) C terminus (Research Diagnostics, Flanders, New Jersey), (2) rabbit polyclonal antibodies to plakoglobin (Pg) N terminus (H80, Santa Cruz Biochnology, Santa Cruz, California), (3) mouse monoclonal antibody to plakophilin1 (Pp1) N terminus (5C2, PROGEN, Heidelberg, Germany), (4) mouse monoclonal antibody to mouse desmoglein1 (Dsg1) C terminal side of intracellular domain (DG3.10, Research Diagnostics, Flanders, New Jersey), (5) guinea pig polyclonal antibodies to desmocollin3 (Dsc3) N terminal side of intracellular domain (gp2280, a kind gift from Dr. P.J. Koch) [11], (6) guinea pig polyclonal antibodies to mouse desmocollin1 (Dsc1) N terminal side of intracellular domain (gp899, a kind gift from Dr. P.J. Koch) [11], (7) mouse monoclonal antibody to mouse desmoglein3 (Dsg3) extracellular domain (AK18) [12]. The dilutions of the antibodies for post-embedding immunogold-EM were: (1) 1:40, (2) 1:40, (3) 1:4, (4) 1:40, (5) 1:400, (6) 1:100 and (7) 1:2.

### 2.3. Post-embedding immunogold-EM

Post-embedding immunogold-EM with cryofixation and freeze substitution without using chemical fixatives was performed as previously described [13]. In brief, samples were taken from the oral mucous membrane of mice and rapidly frozen by plunging them into liquid propane cooled to -190 °C. The samples were substituted in methanol at -60 °C for 48 h, embedded in Lowicryl K11M (Chemische Werke Lowi, Waldkraiburg, Germany) at -60 °C

and polymerized by UV radiation. Ultrathin sections were cut from the samples and sequentially incubated with blocking buffer, 5% normal goat serum (NGS), 0.8% bovine serum albumin (BSA), 0.1% gelatin and 2 mM NaN<sub>3</sub> in phosphate-buffered saline (PBS) pH 7.4, for 30 min at room temperature, and primary antibodies diluted in incubation buffer (PBS pH 7.4 with 1% NGS, 0.8% BSA, 0.1% gelatin and 2 mM NaN<sub>3</sub>) for overnight at 4 °C. After washing with washing buffer (PBS pH 7.4 with 0.8% BSA, 0.1% gelatin and 2 mM NaN<sub>3</sub>), the sections were incubated with 5-nm gold-conjugated secondary antibodies (anti-rabbit or anti-mouse IgG (H + L), Amersham Bioscience, Buckinghamshire, UK; anti-guinea pig IgG (H + L), BB International, London, UK) diluted 1:40 in incubation buffer (PBS pH 7.4 with 1% NGS, 0.8% BSA, 0.1% gelatin and 2 mM NaN<sub>3</sub>) overnight and then washed with washing buffer and distilled water. To enlarge the gold particles, the sections were incubated with the IntenSE silver enhancement solutions (Amersham Bioscience) for 3 min as described previously [14]. Sections were counterstained with uranyl acetate and lead citrate and observed under the transmission EM (model 1200EX, JEOL, Tokyo, Japan). All the immunoEM studies were duplicated using two different mice.

### 2.4. Quantitative analysis

In order to detect early molecular changes before desmosome splitting occurred, all the samples were from normal appearing mucous membranes. Desmosomes between the basal cells and suprabasal cells (apical desmosomes, i.e., desmosomes in the apical side of basal cells) and desmosomes between the spinous cells in the mid-epidermis were analyzed separately because the normal molecular composition of a desmosome may differ according to the different cell layer. EM figures of desmosomes that were cut perpendicularly to the plasma membrane so that three layers of each plasma membrane were clearly seen were selected and statistically analyzed.

For the analysis of the distribution of desmosomal components, the distance of each gold particle from the outermost layer of the plasma membrane was measured on the electron micrographs as shown in Fig. 1 and plotted on a histogram as described previously [15]. The mean distances from the plasma membrane were compared statistically with normal controls.

At the same time, the number of the gold particles per desmosome was counted. For each molecule, the mean number of gold particles per desmosome was tested statistically with a *p*-value less than 0.01. In each study, either Student's *t*-test or Welch's *t*-test were used.

As for Dsg3 in the PV model mice, we could not analyze either the distribution or the number, due to the fact that *in vivo* anti-Dsg3 IgG is already bound to Dsg3.

## 3. Results

### 3.1. In Dsg3<sup>-/-</sup> mice, Dp was shifted slightly to the intercellular side and the number of Pg per desmosome was significantly decreased

The structure of the desmosomes seemed to be intact in all samples and no splitting of the desmosome and widening of the intercellular spaces were observed. The ultrastructural localization of Dp, Pg, Pp1, Dsg1, Dsc3 and Dsg3 in the apical desmosomes in the Dsg3<sup>-/-</sup> mouse and its control mouse are shown in Fig. 2(A–J, M–N). Dsg3 was undetectable in the Dsg3<sup>-/-</sup> mouse at all. Dsc1 was undetectable in the apical desmosomes. The localizations of gold particles seemed to show no big difference at a glance between the Dsg3<sup>-/-</sup> and control mouse. The distance of the gold particles labeling from the plasma membrane was plotted (Fig. 3 left panels) and statistical data such as the mean distance, standard error and standard deviation were calculated (Table 1). The mean

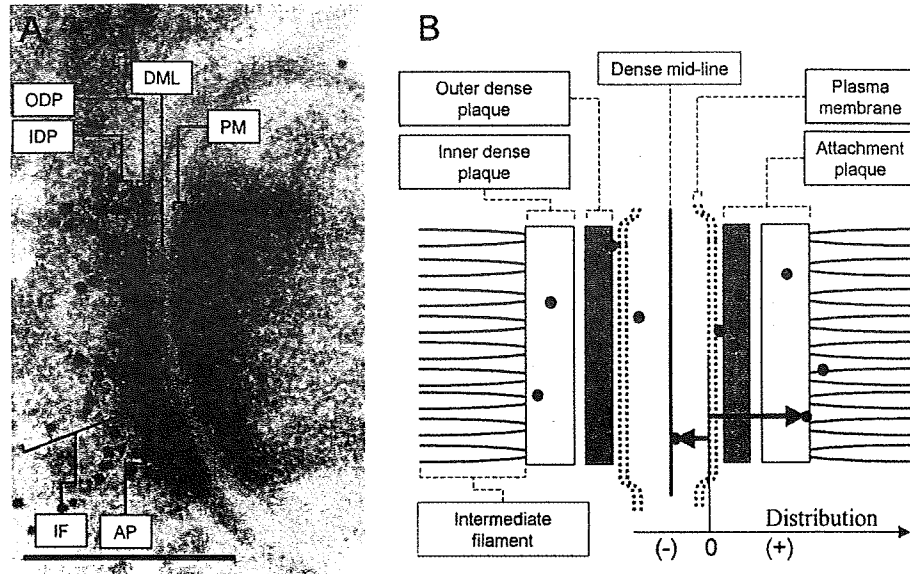


**Fig. 1.** Immunoelectron micrograph of a desmosome (A) and a schematic diagram of a desmosome (B). The ultrastructure of a desmosome using cryofixation and the freeze substitution method was demonstrated. A desmosome has a symmetrical structure that has a dense mid line (DML) as the axis. The gold labels were seen as black dots in the immunoelectron micrograph. For the distribution analysis, the distances of each gold particle were measured from the outer layer of the nearer plasma membrane (PM), and particles lying over the extracellular region were assigned a negative value. ODP, outer dense plaque; IDP, inner dense plaque; AP, attachment plaque; IF, intermediate filament. Bar = 200 nm.

distribution of Dp in the apical desmosomes in *Dsg3*<sup>-/-</sup> mouse was shown to shift 12.6 nm in the intracellular direction in comparison to the control mouse ( $p < 0.05$ ), but the distribution of other desmosomal components was almost identical to that of the control mouse.

In the desmosomes between the spinous cells in the mid-epidermis, Dsc1 were detectable in the desmosome in addition to the components observed in the apical desmosomes (Fig. 2K and L). The distribution of gold particles labeling each component is shown in the right panels of Fig. 3. As shown in Table 1, the mean distribution of Dp in the mid-epidermal desmosomes in the *Dsg3*<sup>-/-</sup> mouse was shown to shift 9.0 nm in the intracellular direction in comparison to the control mouse ( $p < 0.05$ ) but the other components including Dsc1 showed an almost identical distribution.

**Table 1**

The distance of desmosomal components from the plasma membrane in *Dsg3*<sup>-/-</sup> mice.

	Mean $\pm$ SE nm ( $\sigma$ , n)	
	<i>Dsg3</i> <sup>-/-</sup> apical	Control apical
Dp	79.1 <sup>*</sup> $\pm$ 1.4 ( $\sigma = 37.2$ , n = 591)	66.5 <sup>*</sup> $\pm$ 1.6 ( $\sigma = 31.9$ , n = 405)
Pg	29.5 $\pm$ 1.7 ( $\sigma = 24.0$ , n = 196)	26.5 $\pm$ 1.4 ( $\sigma = 22.2$ , n = 254)
Pp1	6.95 $\pm$ 0.78 ( $\sigma = 10.2$ , n = 167)	7.34 $\pm$ 0.79 ( $\sigma = 11.1$ , n = 197)
Dsg1	22.6 $\pm$ 1.1 ( $\sigma = 16.7$ , n = 246)	20.2 $\pm$ 1.0 ( $\sigma = 16.9$ , n = 268)
Dsc3	14.2 $\pm$ 1.0 ( $\sigma = 16.5$ , n = 301)	13.6 $\pm$ 0.8 ( $\sigma = 14.3$ , n = 331)
	Mean $\pm$ SE nm ( $\sigma$ , n)	
	<i>Dsg3</i> <sup>-/-</sup> middle	Control middle
Dp	74.3 <sup>*</sup> $\pm$ 1.2 ( $\sigma = 34.4$ , n = 771)	65.3 <sup>*</sup> $\pm$ 1.3 ( $\sigma = 32.1$ , n = 579)
Pg	26.2 $\pm$ 1.2 ( $\sigma = 23.4$ , n = 372)	25.1 $\pm$ 1.1 ( $\sigma = 21.7$ , n = 394)
Pp1	6.93 $\pm$ 0.65 ( $\sigma = 12.3$ , n = 356)	7.96 $\pm$ 0.72 ( $\sigma = 12.6$ , n = 304)
Dsg1	20.2 $\pm$ 0.8 ( $\sigma = 15.1$ , n = 337)	22.3 $\pm$ 0.9 ( $\sigma = 16.2$ , n = 320)
Dsc3	7.98 $\pm$ 0.69 ( $\sigma = 12.7$ , n = 337)	7.52 $\pm$ 0.62 ( $\sigma = 11.4$ , n = 344)
Dsc1	8.21 $\pm$ 0.72 ( $\sigma = 12.8$ , n = 318)	9.81 $\pm$ 0.69 ( $\sigma = 14.0$ , n = 418)

SE, standard error;  $\sigma$ , standard deviation; n<sub>H</sub>, number of particles used for the analysis; apical, between basal and supra basal.

<sup>\*</sup> Significantly different at  $p < 0.0001$ .

The number of labeled proteins per desmosome was counted in the *Dsg3*<sup>-/-</sup> mouse and the control mouse (Table 2). Interestingly, only the number of Pg showed a significant decrease both in the apical (69%) and the mid-epidermal desmosomes (60%) in the *Dsg3*<sup>-/-</sup> mouse. The number of the other components showed no significant difference.

The replication test using another pair of *Dsg3*<sup>-/-</sup> and control mice showed similar results (data not shown)

**3.2. In the PV model mice, Dp was shifted markedly to intercellular side and the number of Pg per desmosome did not show any difference**

The ultrastructural localization of Dp, Pg and Dsc3 in the apical desmosomes in the PV model mouse is shown in Fig. 4. The localization of gold labels for Dp (A) was seen farther from plasma membrane than that in the control mouse (B). The distance

**Table 2**

The number of desmosomal molecular labelings per desmosome in *Dsg3*<sup>-/-</sup> mice.

	Mean number $\pm$ SE ( $\sigma$ , n)	
	<i>Dsg3</i> <sup>-/-</sup> apical	Control apical
Dp	76.4 $\pm$ 9.6 ( $\sigma = 36.1$ , n = 14)	74.8 $\pm$ 8.9 ( $\sigma = 37.8$ , n = 18)
Pg	19.7 <sup>*</sup> $\pm$ 1.8 ( $\sigma = 9.2$ , n = 27)	28.7 <sup>*</sup> $\pm$ 3.0 ( $\sigma = 13.3$ , n = 20)
Pp1	6.2 $\pm$ 0.7 ( $\sigma = 4.4$ , n = 39)	6.1 $\pm$ 0.9 ( $\sigma = 5.0$ , n = 35)
Dsg1	9.0 $\pm$ 0.8 ( $\sigma = 5.2$ , n = 41)	8.8 $\pm$ 1.0 ( $\sigma = 6.4$ , n = 38)
Dsc3	5.0 $\pm$ 0.4 ( $\sigma = 3.4$ , n = 79)	6.1 $\pm$ 0.4 ( $\sigma = 4.4$ , n = 96)
	Mean number $\pm$ SE ( $\sigma$ , n)	
	<i>Dsg3</i> <sup>-/-</sup> middle	Control middle
Dp	80.6 $\pm$ 5.2 ( $\sigma = 30.7$ , n = 35)	89.9 $\pm$ 8.3 ( $\sigma = 47.5$ , n = 33)
Pg	24.7 <sup>*</sup> $\pm$ 1.4 ( $\sigma = 8.1$ , n = 33)	41.3 <sup>*</sup> $\pm$ 3.0 ( $\sigma = 17.4$ , n = 33)
Pp1	11.9 $\pm$ 0.8 ( $\sigma = 5.9$ , n = 61)	11.3 $\pm$ 1.0 ( $\sigma = 6.5$ , n = 47)
Dsg1	29.7 $\pm$ 3.3 ( $\sigma = 18.2$ , n = 31)	34.7 $\pm$ 2.6 ( $\sigma = 16.2$ , n = 39)
Dsc3	4.0 $\pm$ 0.3 ( $\sigma = 3.2$ , n = 123)	4.9 $\pm$ 0.4 ( $\sigma = 4.0$ , n = 110)
Dsc1	6.0 $\pm$ 0.5 ( $\sigma = 4.6$ , n = 88)	8.3 $\pm$ 0.8 ( $\sigma = 6.7$ , n = 65)

SE, standard error;  $\sigma$ , standard deviation; n, number of desmosomes used for the analysis; apical, between basal and supra basal.

<sup>\*</sup> Significantly different at  $p < 0.0001$ .

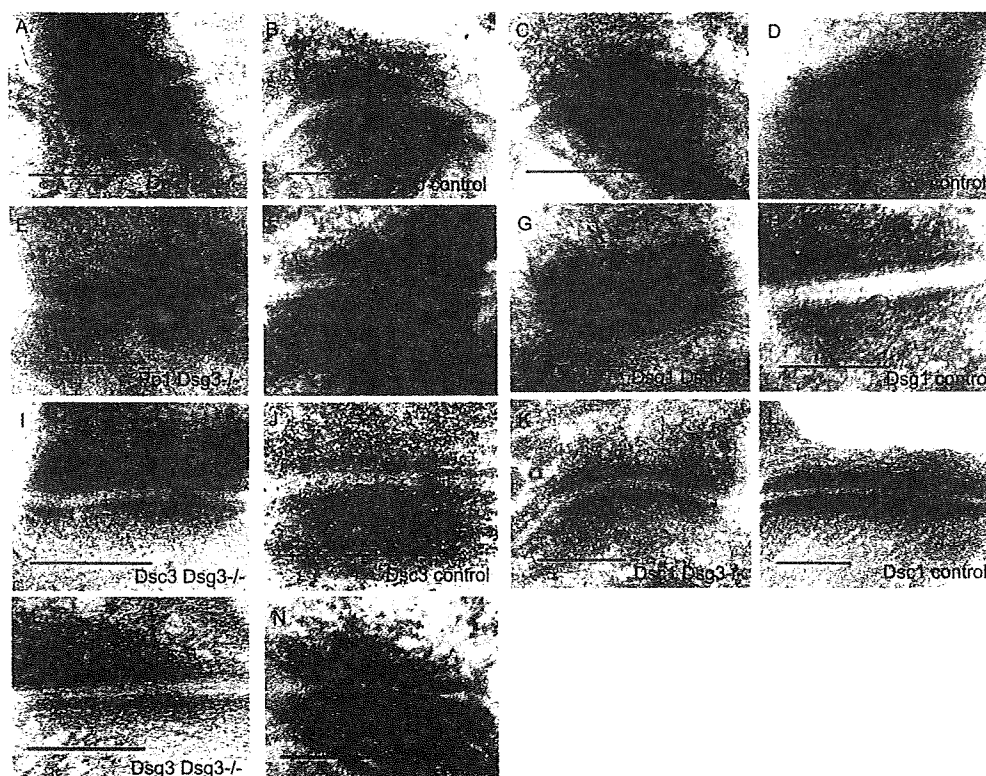


**Fig. 2.** The ultrastructural localization of desmosomal components in the *Dsg3*<sup>-/-</sup> mouse and the control mouse. (A, C, E, G, I and M) were from the desmosomes on the apical side of basal cells in the *Dsg3*<sup>-/-</sup> mouse and (B, D, F, H, J and N) were from the desmosomes on the apical side of basal cells in the control mouse. (K and L) were from desmosomes on the spinous cells in the *Dsg3*<sup>-/-</sup> and the control mouse. The Dp labels (A, B) were seen at the intracellular area distant from plasma membrane (inner dense plaque) in both mice. The Pg labels (C, D) and Dsg1 labels (G, H) were seen on the outer dense plaque. The Pp1 labels (E, F) and Dsc3 labels (I, J) were seen along the plasma membrane of desmosomes. The Dsg3 labels in the desmosomes in the *Dsg3*<sup>-/-</sup> mouse (M) were completely undetectable. On the other hand, the Dsg3 labels in the desmosomes in the control mouse (N) were seen along the plasma membrane. Except for Dsg3, no apparent difference between the two mice was recognized before the statistical analyses were performed. Dsc1 (K, L) in the mid-epidermal desmosomes was observed along the plasma membrane of desmosomes. Bars = 200 nm.

between the gold particles and the plasma membrane was plotted in Fig. 5(left panels). There were two peaks in the Dp distribution of apical desmosomes. One major peak was located at the position identical to that of the control mouse. An additional minor peak was seen at 100 nm more distant from the major peak. The mean distribution of Dp in the apical desmosomes in the PV model mouse shifted 22.7 nm in the intracellular direction (Table 3). The distribution of Pg and Dsc3 showed no locational changes. In the

mid-epidermal desmosomes, Dsc1 was detectable and is shown in Fig. 4(G and H). The distribution of the gold particles labeling each component is shown in the right panels in Fig. 5. As shown in Table 3, the mean distribution of Dp in the mid-epidermal desmosomes in the PV model mouse was shifted 24.2 nm in the cytoplasmic direction ( $p < 0.05$ ). The other components including Dsc1 showed almost identical distribution to that in the control mouse. The number of the gold labeling per desmosome was counted and summarized in Table 4. None of the desmosomal components showed a significant difference between the PV model

**Table 3**

The distance of desmosomal components from the plasma membrane in PV model mice.

	Mean $\pm$ SE ( $\sigma$ , n)	
	PV model apical	Control apical
Dp	94.2 $\pm$ 2.4 ( $\sigma$ = 45.1, n = 354)	71.5 $\pm$ 1.7 ( $\sigma$ = 34.7, n = 443)
Pg	23.7 $\pm$ 1.2 ( $\sigma$ = 16.6, n = 188)	24.5 $\pm$ 1.1 ( $\sigma$ = 15.8, n = 226)
Dsc3	13.6 $\pm$ 0.9 ( $\sigma$ = 13.7, n = 238)	12.1 $\pm$ 0.7 ( $\sigma$ = 12.7, n = 288)
	Mean $\pm$ SE ( $\sigma$ , n)	
	PV model middle	Control middle
Dp	93.0 $\pm$ 2.0 ( $\sigma$ = 40.5, n = 423)	68.8 $\pm$ 1.5 ( $\sigma$ = 32.8, n = 484)
Pg	26.0 $\pm$ 0.8 ( $\sigma$ = 15.4, n = 348)	24.5 $\pm$ 0.9 ( $\sigma$ = 16.2, n = 302)
Dsc3	8.10 $\pm$ 0.50 ( $\sigma$ = 9.9, n = 387)	9.41 $\pm$ 0.66 ( $\sigma$ = 10.9, n = 273)
Dsc1	8.36 $\pm$ 0.53 ( $\sigma$ = 10.6, n = 394)	8.49 $\pm$ 0.54 ( $\sigma$ = 10.8, n = 408)

SE, standard error;  $\sigma$ , standard deviation; n, number of particles used for the analysis; apical, between basal and supra basal.

\* Significantly different at  $p < 0.0001$ .

**Table 4**

The number of desmosomal molecular labelings per desmosome in PV model mice.

	Mean number $\pm$ SE ( $\sigma$ , n)	
	PV model apical	Control apical
Dp	51.2 $\pm$ 4.9 ( $\sigma$ = 21.3, n = 19)	48.6 $\pm$ 4.7 ( $\sigma$ = 18.9, n = 16)
Pg	34.8 $\pm$ 1.9 ( $\sigma$ = 7.8, n = 17)	32.8 $\pm$ 2.6 ( $\sigma$ = 12.6, n = 23)
Dsc3	4.2 $\pm$ 0.3 ( $\sigma$ = 2.5, n = 65)	4.3 $\pm$ 0.3 ( $\sigma$ = 2.8, n = 72)
	Mean number $\pm$ SE ( $\sigma$ , n)	
	PV model middle	Control middle
Dp	49.6 $\pm$ 5.0 ( $\sigma$ = 27.2, n = 30)	49.2 $\pm$ 4.0 ( $\sigma$ = 21.3, n = 29)
Pg	38.7 $\pm$ 3.3 ( $\sigma$ = 16.3, n = 25)	39.9 $\pm$ 3.0 ( $\sigma$ = 15.8, n = 29)
Dsc3	5.6 $\pm$ 0.3 ( $\sigma$ = 3.4, n = 132)	4.6 $\pm$ 0.4 ( $\sigma$ = 3.7, n = 91)
Dsc1	7.3 $\pm$ 0.7 ( $\sigma$ = 5.3, n = 51)	5.9 $\pm$ 0.7 ( $\sigma$ = 5.6, n = 56)

SE, standard error;  $\sigma$ , standard deviation; n, number of desmosomes used for the analysis; apical, between basal and suprabasal.

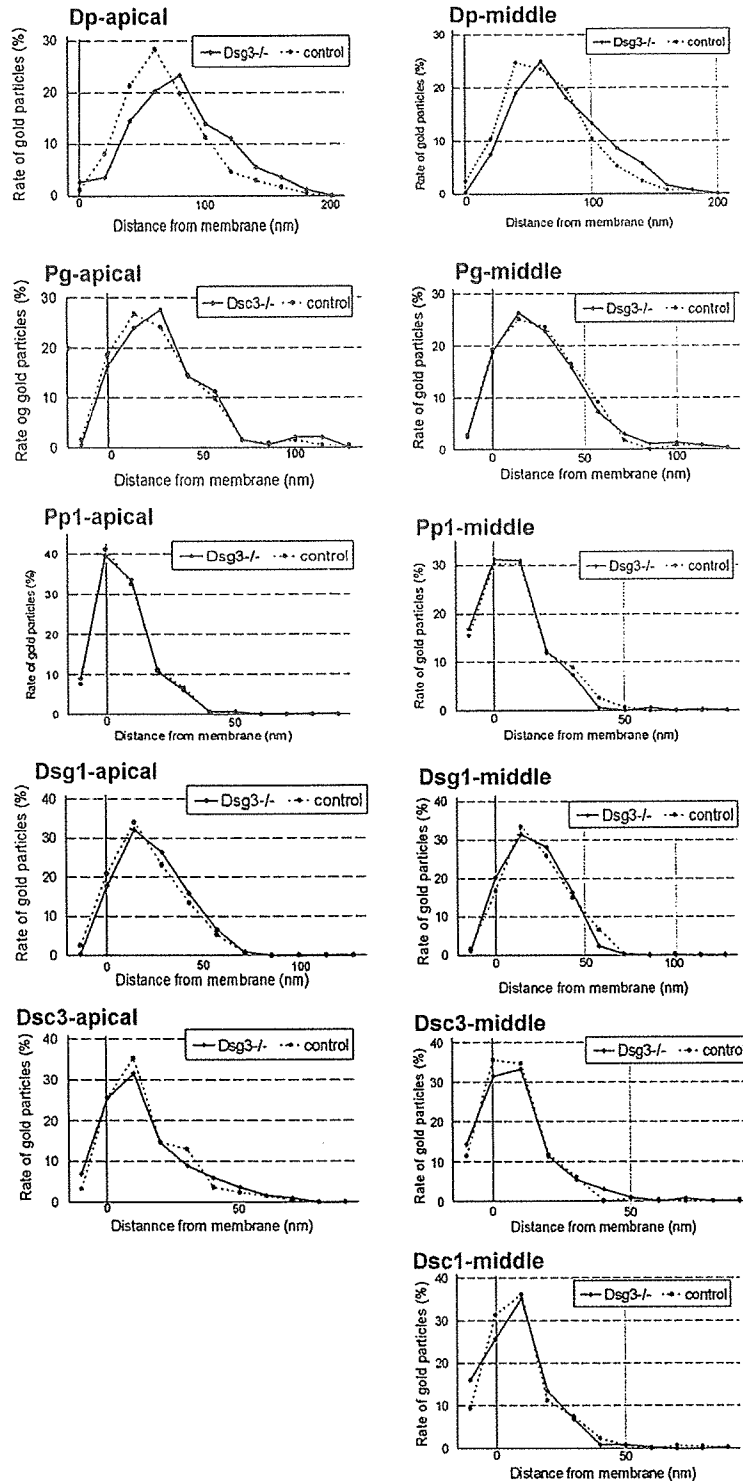


**Fig. 3.** The distribution of desmosomal components in the *Dsg3*<sup>-/-</sup> mouse. The distances between the gold labels and the plasma membrane in the *Dsg3*<sup>-/-</sup> and the control mouse were plotted. The results from apical desmosomes were shown in the left panels, and those from desmosomes in the mid-epidermis were in the right panels. Note the small shifts in the peaks in the Dp distributions. The mean distances are summarized in Table 1.

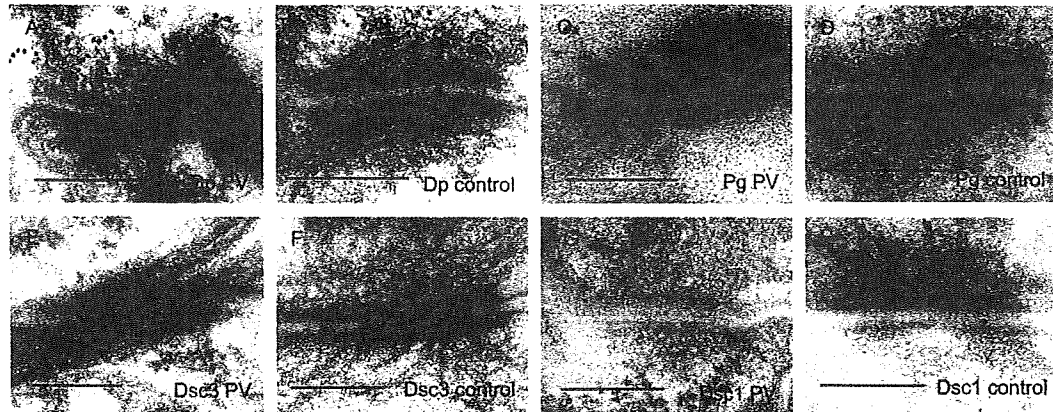


Fig. 4. The ultrastructural localization of the desmosomal components in the PV model mice. (A–F) were from the apical desmosomes in the PV model mice or control. (G and H) were from the mid-epidermal desmosomes. Bars = 200 nm.

mouse and its control mouse in both the apical and mid-epidermal desmosomes.

The replication test using another pair of PV model and control mice showed similar results (data not shown).

#### 4. Discussion

Dp is predicted to form a homodimer containing two globular end domains joined by a central alpha-helical rod domain [16]. The C-terminal domain of Dp interacts with intermediate filaments [17] and the N-terminal domain interacts with Dsc, Pg and Pp1 [18]. On the other hand, Dp cannot bind to Dsg1 or Dsg3 directly, but it binds indirectly via Pg [19,20] (Fig. 6). The findings in this study are summarized in Table 5. The number of Pg in the desmosome was decreased in Dsg3<sup>-/-</sup> mice and this may indicate a close relationship between Dsg3 and Pg. The genetic lack of Dsg3 might influence the recruitment of Pg into desmosomes. In addition, the molecular compensation for Dsg3 by other desmosomal cadherins did not occur in terms of the molecular quantity in the Dsg3<sup>-/-</sup> mouse desmosomes. This fact further confirms that the acantholysis seen in the Dsg3<sup>-/-</sup> mice was due to the fragility of desmosomes that lack Dsg3. However, the PV model mice did not show any change in the number of desmosomal components including Pg. This result indicates that the decrease of Pg does not play a role in the mechanism of acantholysis in the PV model mouse.

There was a small but statistically significant shift of Dp in the intracellular direction in Dsg3<sup>-/-</sup> mice. In other words, the lack of Dsg3 influenced the location of Dp although they are not connected directly. The decreased number of Pg may account for this phenomenon. Although the number of Dp was not reduced, Pg, a major ligand of Dp in the attachment plaque, was decreased and Dp might be dragged toward the cytoplasm. Otherwise, the small shift of Dp might simply be the result of a conformational change of the molecule due to the deficiency of its ligand.

The distribution of Dp in PV model mice was localized much more distant from the plasma membrane than in Dsg3<sup>-/-</sup> mice. From the Dp distribution, there seemed to be two populations of Dp; a non-shifted group and a shifted group, in the apical desmosomes. The shift is estimated to be about 100 nm intracellularly from the normal location, which makes the mean distance 22.7 nm longer than that of the normal control. Because the PV model mice did not show any change in the number of desmosomal components, the mechanisms of the large Dp shift in PV model mice cannot be explained by a decrease of Pg, as in the Dsg3<sup>-/-</sup> mice. Autoantibody binding to Dsg3 in PV model mice should transfer some signals into the cytoplasm and some intracellular events may occur [21–25]. Therefore, the large shift of Dp in the PV model mice might possibly suggest the intrinsic elongation of Dp as a signaling event. However, keratin retraction from the cell membrane after PV antibody binding is a well-known

Table 5

A summary of the desmosomal molecular change in the Dsg3<sup>-/-</sup> and PV model mice in this study.

	Dsg3 <sup>-/-</sup>		PV model	
	Apical	Middle	Apical	Middle
<i>Changes in molecular amount per desmosome</i>				
Dp	-	-	-	-
Pg	31% decrease	40% decrease	-	-
Pp1	-	-	-	-
Dsg1	-	-	-	-
Dsc3	-	-	-	-
Dsc1	-	-	-	-
<i>Changes in molecular localization</i>				
Dp	12.6 nm inside shift	9.0 nm inside shift	22.7 nm inside shift	24.2 nm inside shift
Pg	-	-	-	-
Pp1	-	-	-	-
Dsg1	-	-	-	-
Dsc3	-	-	-	-
Dsc1	-	-	-	-

Apical, between basal and supra basal.

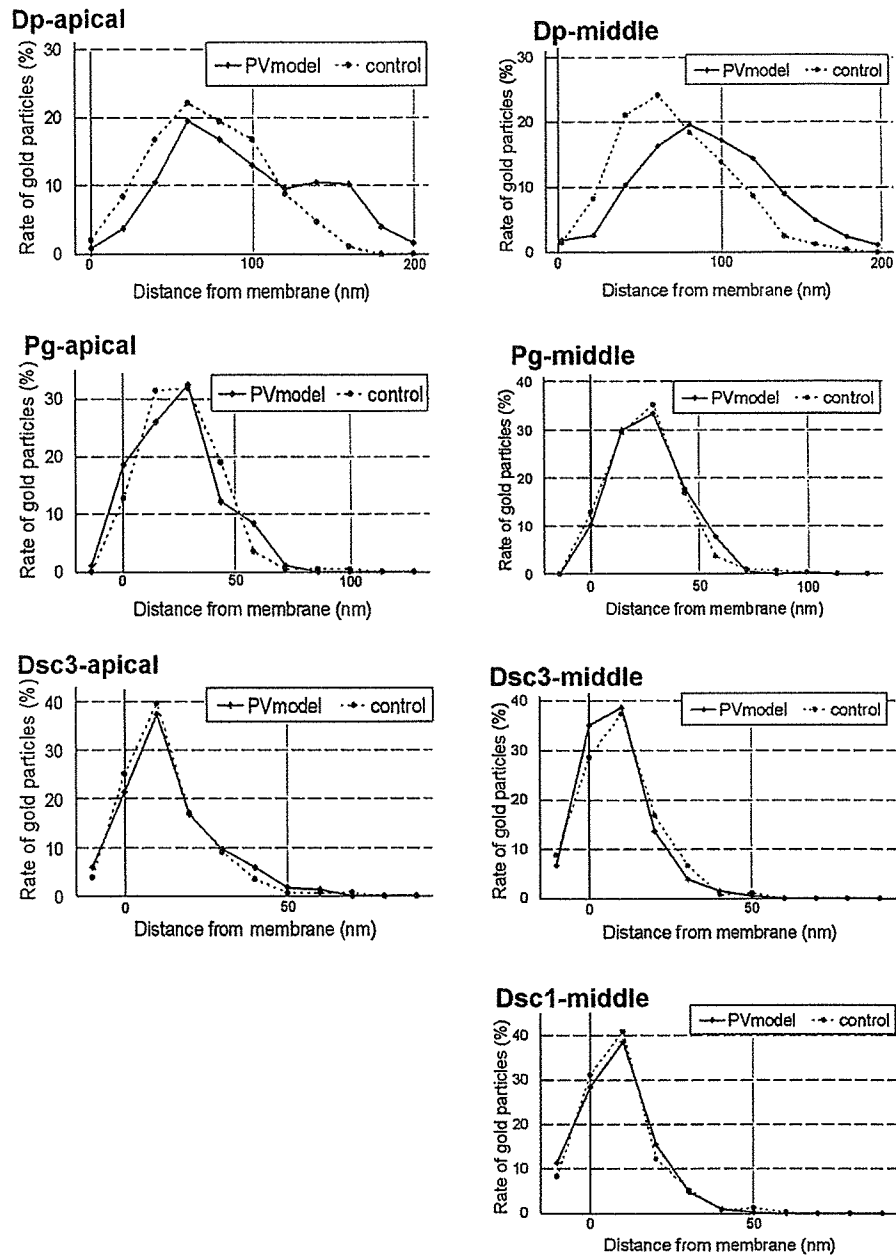


Fig. 5. The distribution of the desmosomal components in the PV model mice and control mouse. The distances between Dp, Pg, Dsc3 and Dsc1 labels and the plasma membrane in the PV model and the control mouse were plotted. The results from apical desmosomes were shown in the left panels, and those from desmosomes in the mid-epidermis were in the right panels. There were two peaks in the Dp distribution of the apical desmosomes. One major peak was located at a position identical to that observed in the control mice. An additional minor peak was seen at 100 nm more distant from the major peak.

*in vitro* phenomenon [7]. Retraction of keratin with Dp is observed at lateral side of basal keratinocytes of the PV model mice [4]. Moreover, a recent report of a model for the disruption of desmosomes in response to PV autoantibodies showed that the Dsg3/Pg complex appears to separate from Dp [9]. Therefore, it is suggested that a large shift of Dp may represent a keratin retraction reactive to autoantibody binding. The desmosomal molecular composition was studied in both the apical and mid-epidermal desmosomes and yielded similar results. Although an apparent minor peak could not be detected in mid-epidermal desmosomes, mean distance of Dp shifted to the similar degree. Considering the fact that the cell separation takes place between the basal and the

suprabasal cells in PV model mice, the shift of Dp alone is not sufficient to explain the mechanism of acantholysis. A recent study demonstrates that the human PV IgG has a direct inhibitory ability against Dsg3-mediated transinteraction [26]. The functional blocking of Dsg3 in the apical desmosomes may be important to explain the cell separation.

In conclusion, this highly detailed EM study detected distinct molecular changes between Dsg3<sup>-/-</sup> mice and PV model mice and indicated that the binding of autoantibodies induced the shift of Dp from the desmosomal plaque, which could be an early molecular change before acantholysis occurs under the *in vivo* conditions of the PV model mouse.

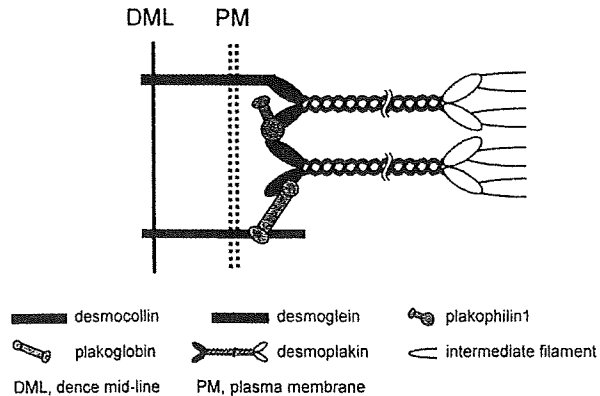


Fig. 6. A schematic molecular model of a desmosome. This model is based on previous yeast two hybrid studies. Dsg does not directly bind to the Dp, but indirectly via Pg.

## Acknowledgments

This work was supported by Health and Labor Sciences Research Grants for Research on Measures for Intractable Diseases, from the Ministry of Health, Labor and Welfare and by Grant-in Aids for Scientific Research and for the Development of Innovative Technology from the Ministry of Education, Culture, Sports, Science and Technology of Japan. We would like to thank Toshihiko Nagai for technical assistance and Dr. James R. McMillan for critical reading of this manuscript.

## References

- [1] Amagai M, Klaus-Kenton V, Stanley JR. Auto antibodies against a novel epithelial adhering in pemphigus vulgaris, a disease of cell adhesion. *Cell* 1991;67:869–77.
- [2] Amagai M, Karpatis S, Prussick R, Klaus-Kovtun V, Stanley JR. Autoantibodies against the amino-terminal cadherin-like binding domain of pemphigus vulgaris antigen are pathogenic. *J Clin Invest* 1992;90:919–26.
- [3] Koch PJ, Mahoney MG, Ishikawa H, Pulkkinen L, Uitto J, Shultz L, et al. Targeted disruption of the pemphigus vulgaris antigen (desmoglein 3) gene in mice causes loss of keratinocyte cell adhesion with a phenotype similar to pemphigus vulgaris. *J Cell Biol* 1997;137:1091–102.
- [4] Amagai M, Tsunoda K, Suzuki H, Nishifuji K, Koyasu S, Nishikawa T. Use of autoantigen-knockout mice in developing an active autoimmune disease model for pemphigus. *J Clin Invest* 2000;105:625–31.
- [5] Ohyama M, Amagai M, Tsunoda K, Ota T, Koyasu S, Hata J, et al. Immunologic and histopathologic characterization of active disease mouse model for pemphigus vulgaris. *J Invest Dermatol* 2002;118:199–204.
- [6] Shimizu A, Ishiko A, Ota T, Tsunoda K, Koyasu S, Amagai M, et al. Ultrastructural changes in mice actively producing antibodies to desmoglein 3

- parallel those in patients with pemphigus vulgaris. *Arch Dermatol Res* 2002;294:318–23.
- [7] Calderali R, de Bruin A, Baunmann D, Suter MM, Gierkamp C, Balmer V, et al. A central role for the armadillo protein plakoglobin in the autoimmune disease pemphigus vulgaris. *J Cell Biol* 2001;153:823–34.
- [8] Shimizu A, Ishiko A, Ota T, Tsunoda K, Amagai M, Nishikawa T. IgG binds to desmoglein 3 in desmosomes and causes a desmosomal split without keratin retraction in a pemphigus mouse model. *J Invest Dermatol* 2004;122:1145–53.
- [9] Calkin CC, Setzer SV, Jennings JM, Summers S, Tsunoda K, Amagai M, et al. Desmoglein endocytosis and desmosome disassembly are coordinated responses to pemphigus autoantibodies. *J Biol Chem* 2006;281:7623–34.
- [10] Schulz RJ, Parkes A, Mizoguchi E, Bhan AK, Koyasu S. Development of CD4-CD8- abTCR + NK1.1 + T lymphocytes: thymic selection by self antigen. *J Immunol* 1996;157:4379–89.
- [11] Cheng X, Mihindukulasuriya K, Den Z, Kowalczyk AP, Calkins CC, Ishiko A, et al. Assessment of splice variant-specific functions of desmocollin 1 in the skin. *Mol Cell Biol* 2004;24:154–63.
- [12] Tsunoda K, Ota T, Aoki M, Yamada T, Nagai T, Nagagawa T, et al. Induction of pemphigus phenotype by a mouse monoclonal antibody against the amino-terminal adhesive interface of desmoglein 3. *J Immunol* 2003;170:2170–8.
- [13] Shimizu H, McDonald JN, Kennedy AR, Eady RA. Demonstration of intra- and extracellular localization of bullous pemphigoid antigen using cryofixation and freeze substitution for postembedding immunoelectron microscopy. *Arch Dermatol Res* 1989;281:443–8.
- [14] Shimizu H, Ishida-Yamamoto A, Eady RAJ. The use of silver-enhanced 1-nm gold probes for light and electron microscopic localization of intra- and extracellular antigens in skin. *J Histochem Cytochem* 1992;40:883–8.
- [15] Shimizu A, Ishiko A, Ota T, Saito H, Oka H, Tsunoda K, et al. In vivo ultrastructural localization of the desmoglein 3 adhesive interface to the desmosome mid-line. *J Invest Dermatol* 2005;124:984–9.
- [16] O'Keefe EJ, Erickson HP, Bennett WG. Desmoplakin I and desmoplakin II. Purification and characterization. *J Biol Chem* 1989;264:8310–8.
- [17] Stappenbeck TS, Green KJ. The desmoplakin carboxyl terminus coaligns with and specifically disrupts intermediate filament networks when expressed in cultured cells. *J Cell Biol* 1992;116:197–209.
- [18] Smith EA, Fuchs E. Defining the interactions between intermediate filaments and desmosomes. *J Cell Biol* 1998;141:1229–41.
- [19] Kowalczyk AP, Bornslaeger EA, Borgwardt JE, Palka HL, Dhaliwal AS, Corcoran CM, et al. The amino-terminal domain of desmoplakin binds to plakoglobin clusters desmosomal cadherin-plakoglobin complexes. *J Cell Biol* 1997;139:773–84.
- [20] Green KJ, Gaudry CA. Are desmosomes more than tethers for intermediate filaments? *Nat Rev* 2000;1:208–16.
- [21] Kitajima Y, Aoyama Y, Seishima M. Transmembrane signaling for adhesive regulation of desmosomes and hemidesmosomes, and for cell-cell detachment induced by pemphigus IgG in cultured keratinocytes: involvement of protein kinase C. *J Invest Dermatol Symp Proc* 1999;4:137–44.
- [22] Aoyama Y, Kitajima Y. Pemphigus vulgaris-IgG causes a rapid detection of desmoglein 3(Dsg3) from the Triton X-100 soluble pools, leading to the formation of Dsg3-depleted desmosomes in a human squamous carcinoma cell line, DJM-1 cells. *J Invest Dermatol* 1999;112:67–71.
- [23] Aoyama Y, Owada K, Kitajima Y. A pathogenic autoantibody, pemphigus vulgaris-IgG, induces phosphorylation of desmoglein 3, and its dissociation from plakoglobin in cultured keratinocytes. *Eur J Immunol* 1999;29:2233–40.
- [24] Lo Muzio L, Pannone G, Syaibano S, Mignogna MD, Rubini C, Ruocco E, et al. A possible role of catenin dyslocalization in pemphigus vulgaris pathogenesis. *J Cutan Pathol* 2001;28:460–9.
- [25] Rubenstein DS, Diaz LA. Pemphigus antibody induced phosphorylation of keratinocyte proteins. *Autoimmunity (England)* 2006;39:577–86.
- [26] Heupel WM, Zillikens D, Drenckhahn D, Waschke J. Pemphigus vulgaris IgG directly inhibit desmoglein 3-mediated transinteraction. *J Immunol* 2008;181:1825–34.



\*Alan Lyell Centre for Dermatology, Glasgow, U.K.

†Section of Dermatology, Division of Cancer Sciences and Molecular Pathology,

Robertson Building, University of Glasgow, Glasgow G12 8QQ, U.K.

‡Epithelial Genetics Group, Human Genetics Unit, University of Dundee, Dundee, U.K.

§Section of Infection and Immunology, University of Glasgow, Glasgow, U.K.

¶St John's Institute of Dermatology, St Thomas' Hospital, London, U.K.

E-mail: m.zamiri@clinmed.gla.ac.uk

M. ZAMIRI\*†

F.J.D. SMITH‡

L.E. CAMPBELL‡

L. TETLEY§

R.A.J. EADY¶

M.B. HODGINS†

W.H.I. MCLEAN‡

C.S. MUNRO\*

16 Wan H, Dopping-Hepenstal PJC, Gratian MJ et al. Striate palmoplantar keratoderma arising from desmoplakin and desmoglein 1 mutations is associated with contrasting perturbations of desmosomes and the keratin filament network. *Br J Dermatol* 2004; **150**:878–91.

Key words: autosomal dominant, desmoglein 1, striate palmoplantar keratoderma

Conflicts of interest: none declared.

## References

- Judge MR, McLean WHI, Munro CS. Disorders of keratinisation. In: *Rook's Textbook of Dermatology* (Burns DA, Breathnach SM, Cox NH, Griffiths CEM, eds), 7th edn, Vol. 2. Oxford: Blackwell Publishing, 2004; 34:1–111.
- Rickman L, Simrak D, Stevens HP et al. N-terminal deletion in a desmosomal cadherin causes the autosomal dominant skin disease striate palmoplantar keratoderma. *Hum Mol Genet* 1999; **8**:971–6.
- Hunt DM, Rickman L, Whittock NV et al. Spectrum of dominant mutations in the desmosomal cadherin desmoglein 1, causing the skin disease striate palmoplantar keratoderma. *Eur J Hum Genet* 2001; **9**:197–203.
- Armstrong DKB, McKenna KE, Purkis PE et al. Haploinsufficiency of desmoplakin causes a striate subtype of palmoplantar keratoderma. *Hum Mol Genet* 1999; **8**:143–8.
- Lai-Cheong JE, Arita K, McGrath JA. Genetic diseases of junctions. *J Invest Dermatol* 2007; **127**:2713–25.
- Hershkovitz D, Lugassy J, Indelman M et al. Novel mutations in DSG1 causing striate palmoplantar keratoderma. *Clin Exp Dermatol* 2009; **34**:224–8.
- Dua-Awreth MB, Shimomura Y, Kraemer L et al. Mutations in the desmoglein 1 in five Pakistani families with striate palmoplantar keratoderma. *J Dermatol Sci* 2009; **53**:192–7.
- Hayat MA. Chapter 2. Rinsing, dehydrating and embedding. In: *Principles and Techniques of Electron Microscopy: Biological Applications*. (Hayat MA, eds). Basingstoke: MacMillan Press, 1989; 79–137.
- Whittock NV, Ashton GH, Dopping-Hepenstal PJ et al. Striate palmoplantar keratoderma resulting from desmoplakin haploinsufficiency. *J Invest Dermatol* 1999; **113**:940–6.
- Milingou M, Wood P, Masouye I et al. Focal palmoplantar keratoderma caused by an autosomal dominant inherited mutation in the desmoglein 1 gene. *Dermatology* 2006; **212**:117–22.
- Hamada T, South AP, Mitsuhashi Y et al. Genotype–phenotype correlation in skin fragility–ectodermal dysplasia syndrome resulting in mutations in plakophilin 1. *Exp Dermatol* 2002; **11**:107–14.
- Barber AG, Wajid M, Columbo M et al. Striate palmoplantar keratoderma resulting from a frameshift mutation in the desmoglein 1 gene. *J Dermatol Sci* 2007; **45**:161–6.
- Whittock NV, Smith EJ, Wan H et al. Frameshift mutation in the V2 domain of human keratin 1 results in striate palmoplantar keratoderma. *J Invest Dermatol* 2002; **118**:838–44.
- Wan H, Dopping-Hepenstal PJC, Gratian MJ et al. Desmosomes exhibit site-specific features in human palm skin. *Exp Dermatol* 2003; **12**:378–88.
- Cui Y, Hagan KW, Zhang S, Peltz SW. Identification and characterization of genes that are required for the accelerated degradation of mRNAs containing a premature translational termination codon. *Genes Dev* 1995; **9**:423–36.

## Immunolocalization of Epstein–Barr virus-related antigens in a case of sweat gland adenocarcinoma

DOI: 10.1111/j.1365-2133.2009.09319.x

SIR, Epstein–Barr virus (EBV) is a ubiquitous human herpes virus implicated in the carcinogenesis of several malignant neoplasms. It is thought to play an important pathogenic role in lymphomas<sup>1</sup> and nasopharyngeal carcinoma.<sup>2</sup> Recently, there have been scattered reports linking EBV with conventional epithelial cancers including breast, lung, gastric and renal carcinomas.<sup>3</sup> However, to date, no reports have linked EBV with epithelial skin cancer.

Here we report a 78-year-old Japanese man with a progressively enlarging tumour of the right side of his scrotum of 5-month duration. He had a past history of myocardial infarction and hypertension but no immunodeficiency.

The tumour was a mushroom-shaped reddish mass with a diameter of 17 mm (Fig. 1a). Excisional biopsy was performed. Histopathologically, the tumour was exophytic and was composed of basophilic tumour nests of irregular shape and size. The overlying epidermis was almost absent but had connections to the tumour cells at the periphery of the tumour (Fig. 1b). A few small tubular structures were observed in part of the tumour nest. The tumour cells had hyperchromatic nuclei showing atypia and eosinophilic cytoplasm (Fig. 1c) and were positive for cytokeratin 8/18, carcinoembryonic antigen, epithelial membrane antigen, gross cystic disease fluid protein-15 (GCDFP-15) (Fig. 1d) and periodic acid–Schiff diastase-resistant material. No other internal malignancy was detected by radiological analysis. We diagnosed this tumour as sweat gland adenocarcinoma of the skin because the tumour had connections to the epidermis and no other internal malignancy was detected. Wide resection with a 1 cm normal margin was performed. Two months after the operation, swelling of the right inguinal lymph node was noticed and biopsy revealed metastasis of the adenocarcinoma. Inguinal lymph node dissection was performed and two of 17 lymph nodes were reported to have metastasis of sweat gland adenocarcinoma. No other metastasis was detected by radiological analysis. Almost 4 years after the initial operation there is no sign of recurrence or metastasis. On further analysis of the specimen, the expression of EBV-encoded small RNA was

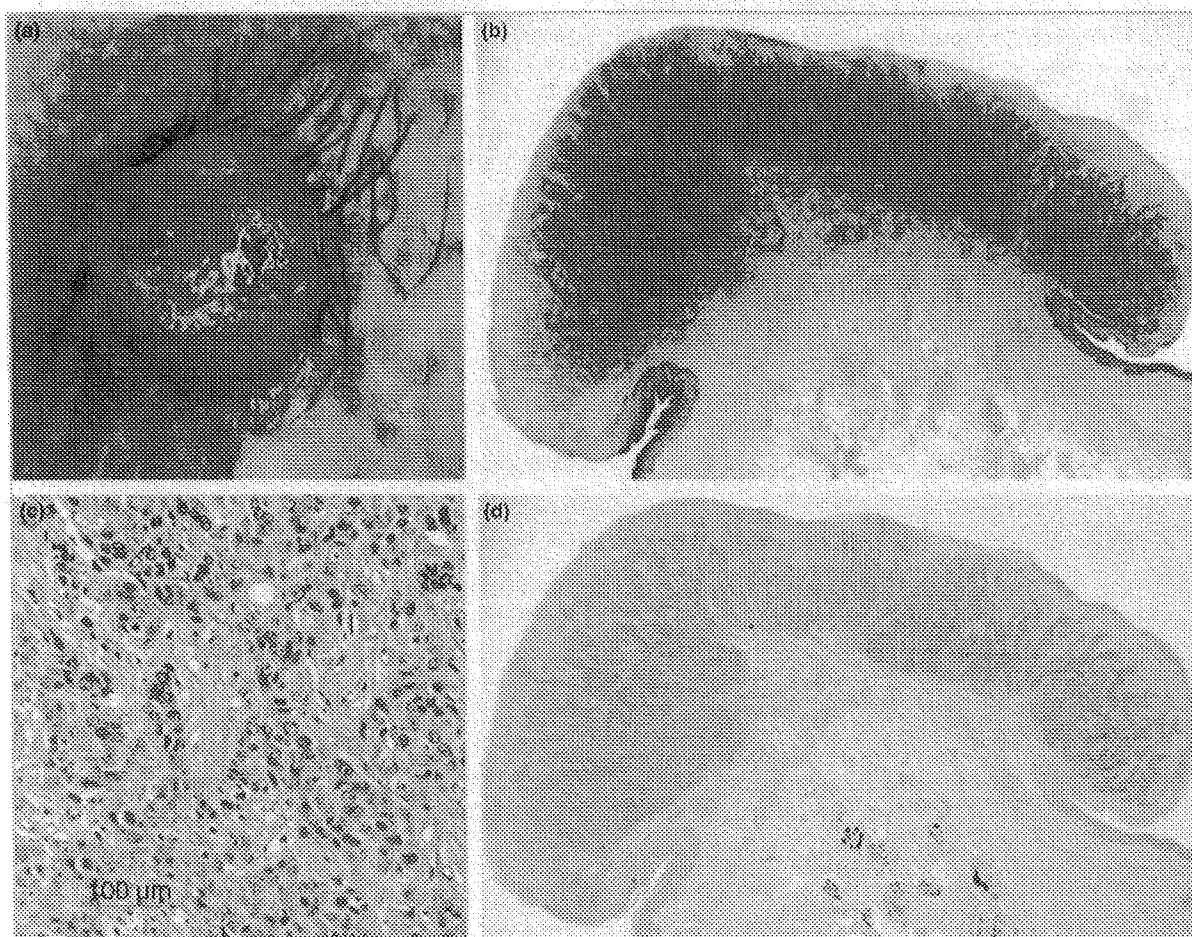


Fig 1. (a) The tumour was a mushroom-shaped reddish mass with a diameter of 17 mm; the tumour surface was eroded and bled easily. (b) The tumour was exophytic and composed of basophilic tumour nests. (c) A few small tubular structures were observed in part of the tumour nest; the tumour cells had hyperchromatic nuclei showing atypia and eosinophilic cytoplasm. (d) The tumour cell expressed gross cystic disease fluid protein-15.

observed on in situ hybridization (Fig. 2a). Also, the expression of EBV-related latent proteins [EBV nuclear antigen (EBNA)-2 (Fig. 2b) and latent membrane protein (LMP)-1 (Fig. 2c)], which are involved in cell transformation, were seen in the tumour. The expression of EBNA-2 (Fig. 2d) was also seen in the metastatic lesion.

Carcinomas derived from sweat glands are grossly divided into two groups. One is a group of tumours resembling their benign counterparts, such as poroma, and named after them, e.g. porocarcinoma, which often occur within the lesion of their respective benign counterpart. The other is a group of tumours which do not have benign counterparts and occur *de novo*. Sweat gland adenocarcinoma belongs to the latter group and is defined as a tumour without any pathological characteristics.<sup>4</sup> Pathogenesis of this neoplasm is not precisely understood, mainly due to the limited number of case reports. It usually appears as a moderate to poorly differentiated adenocarcinoma with regional variation, ranging from true ductule formation to an infiltrative anaplastic cellular zone. It can therefore sometimes be difficult to differentiate

from metastatic carcinoma to the skin with routine haematoxylin and eosin-stained material. In our case, the connection of the tumour cell to the epidermis and the occurrence of metastasis to the lesional lymph nodes may provide strong evidence against metastatic tumour, but the final diagnosis often relies on exclusion of an extracutaneous primary adenocarcinoma by meticulous systemic evaluation.<sup>5</sup> In the literature sweat gland adenocarcinoma has been classified into that of eccrine origin or apocrine origin, referred to as eccrine sweat gland carcinoma,<sup>6</sup> apocrine adenocarcinoma<sup>7</sup> or related syndromes. Eccrine sweat gland carcinoma usually occurs on the head, neck and extremities<sup>6</sup> whereas apocrine adenocarcinoma usually occurs on the axilla and genital skin.<sup>7</sup> Other reports show that GCDFP-15 may be a marker of sweat gland carcinoma of apocrine origin,<sup>8</sup> however, it is often difficult to differentiate sweat gland adenocarcinomas into eccrine or apocrine types only from immunohistochemistry. In our case, localization of the tumour and positive staining for GCDFP-15 suggested that this tumour may have originated from the apocrine gland; however, we could not detect morphological features suggesting an

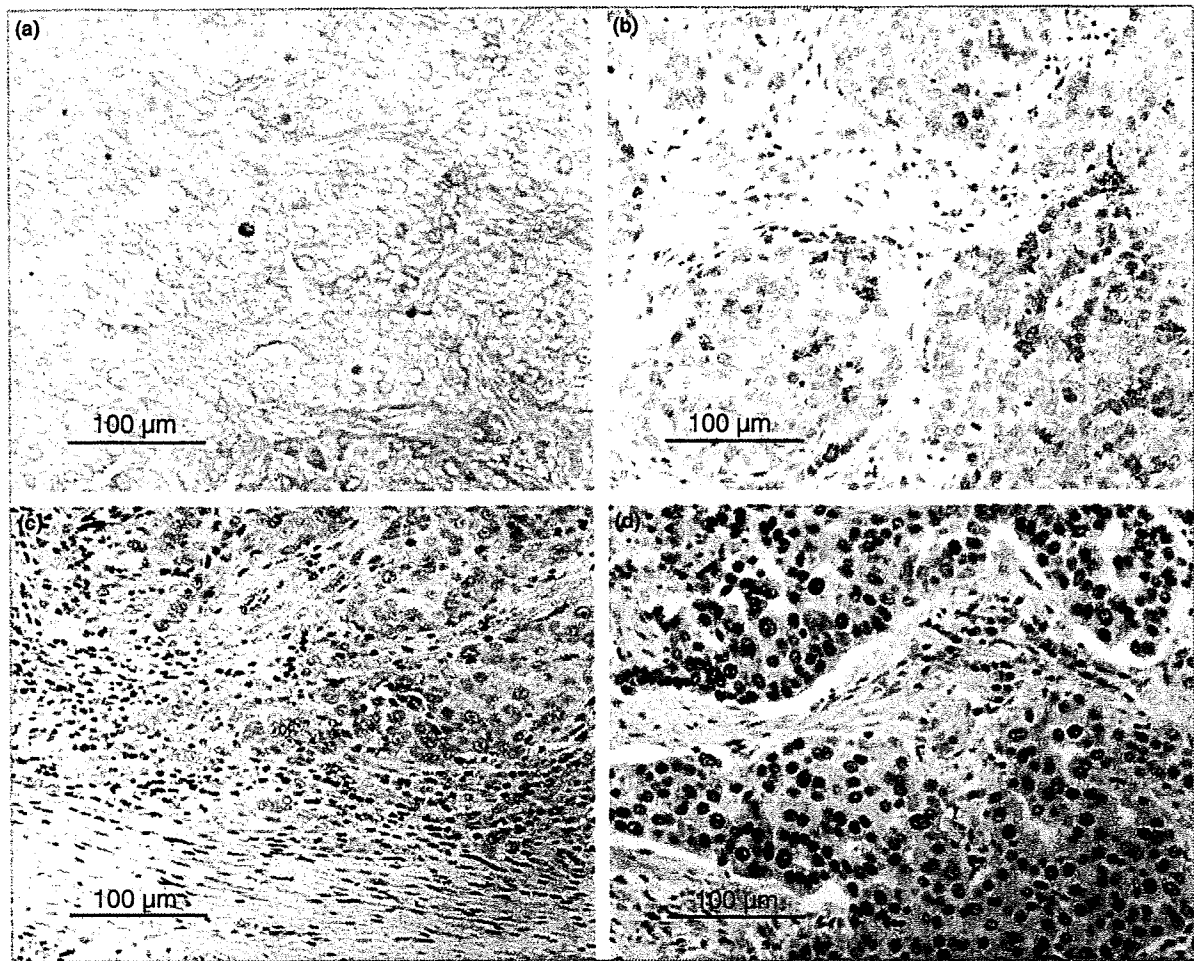


Fig 2. Expressions of Epstein-Barr virus (EBV)-related mRNA and proteins in tumour cells. (a) Signal expression of EBV-encoded small RNA in nuclei of tumour cells; (b) expression of EBV nuclear antigen (EBNA)-2; (c) expression of latent membrane protein (LMP)-1; (d) expression of EBNA-2 in the tumour cells of a metastatic lesion.

apocrine origin, such as decapitation secretion in the specimen sufficient to conclude the origin of this tumour.

The expression of EBV-related latent proteins EBNA-2 and LMP-1 in our case suggests a novel possibility of the role of EBV infection in the pathogenesis of sweat gland adenocarcinoma. EBNA-2 is a transcriptional coactivator that coordinates viral gene expression and also transactivates many cell genes while playing a critical role in cell immortalization.<sup>9</sup> LMP-1 directly links to oncogenesis by virtue of its ability to recruit an array of cellular genes, such as nuclear factor- $\kappa$ B, c-Jun NH2-terminal kinase and p38 mitogen-activated protein kinase.<sup>10</sup> We should pay more attention to EBV in skin cancer and accumulate cases in order not only to clarify its pathogenesis, but also to suggest treatment and disease prevention.

### Acknowledgment

Grant-in-Aid was received from the Ministry of Education, Culture, Sports, Science and Technology of Japan.

\*Departments of Pathology,

†Dermatology and

‡Plastic and Reconstruction Surgery,

School of Medicine, Keio University,

35 Shinanomachi,

Shinjuku-ku, Tokyo, 160-8582, Japan

E-mail: tanese@2001.jukuin.keio.ac.jp

K. TANESE\*†

A. ISHIKO†

K. HAYASE\*

T. YOSHIDA†

K. KISHI‡

T. YAMADA\*

### References

- 1 Jones J, Shurin S, Abramowsky C et al. T-cell lymphomas containing Epstein-Barr viral DNA in patients with chronic Epstein-Barr virus infections. *N Engl J Med* 1988; **318**:733-41.
- 2 Vasef M, Ferlito A, Weiss L. Nasopharyngeal carcinoma, with emphasis on its relationship to Epstein-Barr virus. *Ann Otol Rhinol Laryngol* 1997; **106**:348-56.
- 3 Wang Y, Xue SA, Hallden G et al. Virus-associated RNA I-deleted adenovirus, a potential oncolytic agent targeting EBV-associated tumors. *Cancer Res* 2005; **65**:1523-31.
- 4 Chintamani, Sharma R, Badran R et al. Metastatic sweat gland adenocarcinoma: a clinic-pathological dilemma. *World J Surg Oncol* 2003; **1**:13.

- 5 Yugueros P, Kane WJ, Goellner JR. Sweat gland carcinoma: a clinicopathologic analysis of an expanded series in a single institution. *Plast Reconstr Surg* 1998; **102**:705–10.
- 6 Voutsadakis IA, Bruckner HW. Eccrine sweat gland carcinoma: a case report and review of diagnosis and treatment. *Conn Med* 2000; **64**:263–6.
- 7 Chamberlain RS, Huber K, White JC et al. Apocrine gland carcinoma of the axilla: review of the literature and recommendations for treatment. *Am J Clin Oncol* 1999; **22**:131–5.
- 8 Miyamoto T, Hagari Y, Inoue S et al. Axillary apocrine carcinoma with benign apocrine tumours: a case report involving a pathological and immunohistochemical study and review of the literature. *J Clin Pathol* 2005; **58**:757–61.
- 9 Wensing B, Farrell PJ. Regulation of cell growth and death by Epstein–Barr virus. *Microbes Infect* 2000; **2**:77–84.
- 10 Eliopoulos AG, Gallagher NJ, Blake SM et al. Activation of the p38 mitogen activated protein kinase pathway by Epstein–Barr virus-encoded latent membrane protein 1 coregulates interleukin-6 and interleukin-8 production. *J Biol Chem* 1999; **274**:16085–96.

Key words: Epstein–Barr virus, EBER, EBNA-2, LMP-1, sweat gland adenocarcinoma

Conflicts of interest: none declared.

## Optimizing technique in elliptical excisional surgery: some pearls for practice

DOI: 10.1111/j.1365-2133.2009.09312.x

STR, Proficient technique when performing classic elliptical (fusiform) excisions is a fundamental skill required by dermatologists. The importance of correct design of an ellipse (which most commonly bears a 3 : 1 length to width ratio with a 30° angle at the apices) is emphasized in most if not all basic dermatological surgical texts. When designed and performed correctly, closure of the elliptical defect forms a smooth linear suture line, with no standing cutaneous deformities. Having taught introductory surgical skills to a large number of dermatology trainees, general practitioners and specialist nurses, we have found a number of practical 'surgical pearls' relating to this type of excision to be of benefit in optimizing the outcome of elliptical excisional surgery.

Prior to removing a lesion, it is our standard practice to mark the visible clinical extent of the lesion meticulously in good light using magnification (Fig. 1a). This pivotal step may often be neglected. A dotted line is placed around the periphery of the lesion, and a continuous line marked outside this to delineate the required margins, most commonly 4 mm for excision of the majority of nonmelanoma skin cancers on the trunk and limbs<sup>1</sup> (Fig. 1b). A routine such as this encourages a clear definition of excision margins and enables both the operator and patient to appreciate fully the size of the defect that will be closed and subsequently the length of the resultant scar. We have demonstrated by serial auditing that such a routine greatly reduces

the rate of incomplete excision of lesions, independent of the level of expertise of the operator.

A surgical marker pen is routinely used to delineate the ellipse to be excised. The simple addition of lines at this stage, perpendicular to the long axis of the ellipse, act as a guide to facilitate optimal subcuticular suture placement (Fig. 1c,d) when closing the defect. Although of benefit when operating at any site, we find this practice has particular value on the upper back, as following removal of the ellipse there is a tendency for the wound edges to separate in the vertical plane (medial wound edge inferiorly, lateral wound edge superiorly, for example). The lines thus enable a correct realignment of the tissues optimizing wound closure.

Our practice differs from a similar described technique<sup>2</sup> in that it takes place prior to commencing surgery and does not require the help of a scrubbed assistant. Furthermore, as the lines are delineated prior to surgery, they are oriented to ensure scar placement within relaxed skin tension lines thereby obviating the need for skin hooks in the apices of the defect to ensure correct placement of the lines. Furthermore the extension of these lines outside the margins of the ellipse allows those starting off in the field to visualize the anticipated degree of undermining around the defect which will be needed to create a 'tension-free' closure and can thus be varied in length. The lines also act as a useful guide delineating the lateral extent of the expected operative field, of particular use when other members of the team, such as the surgical assistant, anaesthetize the area.

Under certain circumstances when the best orientation of an ellipse may be difficult to ascertain prior to removal of a lesion, the technique of excising lesions initially as a disc can be useful. Such a method allows any local skin tensions that exist, to create an oval from the original circular defect that has been created. The correction of standing cutaneous deformities along the apices of the oval may then be performed. This technique prevents the tendency to excise a lesion narrowly, simply to close a predesigned ellipse. However, there are caveats to this technique – when free margins are involved or, for example, when operating on the upper back with the patient prone with their arms in front of them. Under the latter circumstance local skin tensions may well be very different from those when the patient is upright.

Orientation of an elliptical specimen may often be neglected, but is essential for identifying correctly the location of residual tumour in the event of an incomplete excision. We routinely orient specimens by 'blunting' one end of the ellipse-shaped specimen, thus obviating the need for a marking suture (Fig. 1e).

Placement of subcuticular sutures to ensure perfect wound edge apposition and eversion and to create a good seal is necessary for the best possible aesthetic result. When closing a larger wound under more tension, the central buried subcuticular suture may slip before being locked, especially when operating without an assistant. We commonly use a 'side-by-side' subcutaneous suture in the centre of the wound to avoid this potential problem. A standard buried